UNC-45 assisted myosin folding depends on a conserved FX_3HY motif implicated in Freeman Sheldon Syndrome

Antonia Vogel[1,5], Renato Arnese[1,5], Ricardo M. Gudino Carrillo[1,2], Daria Sehr[1,4], Andrzej Bylicki[11], Anton Meinhart[1], Tim Clausen[1,3,*]

[1]Research Institute of Molecular Pathology, Vienna BioCenter, Vienna, Austria

[2]Current address: Vienna BioCenter Core Facilities, Vienna, Austria

[3]Vienna BioCenter Core Facilities, Vienna, Austria

[3]Medical University, Vienna, Austria

[4]Current address:ISTA, Austria

[5]These authors contributed equally

*Correspondence: tim.clausen@imp.ac.at

Keywords: protein quality control, myosin proteostasis, myopathy, molecular chaperones, ubiquitin proteasome system, UNC-45, Myo4, MHC-B, UFD-2, crosslinking mass spectrometry

Summary

Myosin motors are critical for diverse motility functions ranging from cytokinesis and endocytosis to muscle contraction. The UNC-45 chaperone controls myosin function mediating the folding, assembly, and degradation of the muscle protein. Here, we analyze the molecular mechanism of UNC-45 as a hub in myosin quality control. We show that UNC-45 forms discrete complexes with folded and unfolded myosin, forwarding them to downstream chaperones and E3 ligases. Structural analysis of a minimal chaperone:substrate complex reveals that UNC-45 binds to a conserved FX_3HY motif in the myosin motor domain. Disrupting the observed interface by mutagenesis prevents myosin maturation leading to protein aggregation in vivo. We also show that a mutation in the FX_3HY motif linked to the Freeman Sheldon Syndrome impairs UNC-45 assisted folding, reducing the level of functional myosin. These findings demonstrate that a faulty myosin quality control is a critical yet unexplored cause of human myopathies.

Introduction

Muscle contraction relies on the sliding of actin and myosin filaments against each other. For efficient power generation, the two myofilaments are arranged in a quasi-crystalline manner in the sarcomere, the basic building block of all muscle cells[1]. Maintaining the higher-order organization of the sarcomere during exercise, proteotoxic stress, and ageing is of utmost importance, as reflected by the many myopathies connected with sarcomeric components[2]. To prevent damage and to oversee the highly specialized proteome of muscle cells, an extended set of molecular chaperones is employed[3]. Abundance and functional diversity of the involved folding factors reflect the intricate structures and assembly pathways of muscle proteins, such as myosin[3,4]. Notably, despite containing an ATPase domain that poses grand challenges for the cellular chaperone machinery[5,6], myosin is the most abundant protein in muscle cells, accounting for about 16% of the entire proteome[7].

Both the folding of myosin and the formation of thick filaments rely on the activity of multiple assembly factors[8], including members of the general chaperone machinery (e.g. HSP70, HSP90 and TRiC), but also muscle cell-specific chaperones. Genetic screens have identified UNC-45 as an essential regulator of myosin proteostasis[9–12]. In addition to functioning as a folding factor of the myosin motor, UNC-45 can form linear protein chains that provide regular spaced docking sites for HSP70 and HSP90. This molecular assembly line allows for coordinated chaperone activity on myosin heads protruding from the thick filament[13]. The important role of UNC-45 for myosin filament formation and sarcomere integrity is reflected by detrimental phenotypes upon genetic disruption. Knock-out of UNC-45 results in embryonic lethality, and both its upregulation and downregulation are linked to severe sarcomere defects[14,15]. Consistent with these findings, UNC-45 mutations have been directly linked to human myopathies [16,17].

UNC-45, which is present in all eukaryotes, employs a UCS domain to interact with myosin, a central domain that mediates oligomerization, and a TPR domain that interacts with members of the protein quality control (PQC) network[18]. The HSP70/HSP90 chaperones bind to the TPR-domain and are required for myosin assembly during muscle development[11,19]. In addition to coordinating filament formation, UNC-45 maintains the level of functional myosin in mature muscle cells

during stress situations. To fulfill this role, UNC-45 uses its TPR domain to interact with the ubiquitin ligase UFD-2, enabling the E3 enzyme to selectively target and ubiquitinate aberrant myosin molecules[20]. Consistent with this quality control function, stress situations applied to muscle tissues induce the interaction of UNC-45 with already assembled myosin molecules[21], whereas knockdown of UNC-45 results in an increase of myosin levels in the sarcomere[22]. However, the mechanism by which the chaperone distinguishes between folding competent and severely damaged myosin proteins and how it channels these into folding and degradation pathways is not understood. Moreover, and in contrast to the well-characterized general chaperones HSP70, HSP90, and TRIC [23–26], little is known about the substrate targeting mechanism of specialized folding factors such as UNC-45. Therefore, studying the interplay between UNC-45 and myosin is not only important to better understand how triage decisions are made in the PQC system but also to delineate the mode of action of client-specific chaperones.

By pursuing an integrative structural biology approach, we reveal that UNC-45 is able to bind myosin present in different conformations. Once bound to UNC-45, the fate of the myosin substrate depends on its folding state. We were able to delineate this mechanism by separating discrete UNC-45 complexes with “folding-competent” or “degradation-prone” myosin, and determining the high-resolution crystal structure of a minimal chaperone:substrate complex. We identified the conserved FX_3HY myosin motif as primary site of UNC-45 interaction and applied cellular assays to demonstrate that this myosin epitope is essential for UNC-45 recruitment and maturation of the muscle protein. Strikingly, a Y582S mutation in this motif is linked to a severe developmental myopathy, the Freeman Sheldon Syndrome (FSS)[27,28]. The site-specific mutation abrogates the interaction between UNC-45 and myosin, causing severe protein misfolding in cells. These data directly relate myosin PQC with myosin-based myopathies, a connection that has not been described and explored so far.

Results

UNC-45 forms separate complexes with folded and unfolded myosin

To characterize the interplay between chaperone and substrate at a molecular level, we reconstituted the complex between *C. elegans* UNC-45 and the motor domain of MHC-B muscle myosin (myo). After co-expression in insect cells, the UNC-45:myo complex was purified by tandem affinity chromatography and size exclusion chromatography (SEC)[20]. In the final SEC run, the UNC-45:myo complex eluted in a reproducible series of high- and low-molecular weight species (**Fig. 1a**). Since the stoichiometry of UNC-45 and myosin was similar in all fractions, the elution peaks likely reflect different conformational states of the bound myosin. To address this point, we compared the SEC elution profiles with those of folded and heat-denatured myosin alone **(Supp. Fig. 1)**. This comparison suggested that the high-molecular weight peak should represent UNC-45 bound to unfolded myosin (UNC-45:myo^{UF}), whereas the second peak contains the chaperone engaged with a mostly folded substrate (UNC-45:myo^{F}). To corroborate the folding state of bound myosin, we took advantage of the lower stability of myosin compared to UNC-45. Myosin, but not UNC-45, unfolds at 27°C allowing us to selectively destabilize myosin at elevated temperature[29]. We thus incubated the two complexes at 4°C and 27°C and reapplied the samples to SEC analysis. For UNC-45:myo^{UF}, the elution volume remained almost unchanged after heat treatment, suggesting that the UNC-45-bound myosin is already unfolded **(Fig. 1b)**. In contrast, when the UNC-45:myo^{F} complex was incubated at 27°C, the reapplied complex shifted to an earlier elution volume, characteristic of the unfolded myosin **(Fig. 1c)**. These data strongly support our notion that myosin in the UNC-45:myo^{F} complex is present in a mostly folded conformation, which is sensitive to heat-induced unfolding.

To identify interacting regions of chaperone and substrate, we performed crosslinking mass spectrometry (XLMS) experiments. Analysis of the UNC-45:myo^{F} complex containing the folded client protein indicated that UNC-45 interlinks can be grouped into two classes **(Fig. 1d Supp. Fig. 2)**. They either comprise residues of predominantly disordered UNC-45 regions (class-I: neck-domain loop 508-524; UCS-loop 602-630; UCS C-terminus 931-961) or residues that are part of structurally well-defined sub-domains (class-II). While class I contacts showed a promiscuous crosslinking pattern, the central part of the UCS-domain (residues 695-720) is

involved in specific class-II contacts via its structurally defined ARM-repeats. Crosslinked residues border the groove of the UCS domain that, based on structural alignment with β-catenin[13], has been suggested to form a myosin-binding canyon. We also observed specific class-II interlinks to the TPR domain of UNC-45, hinting to an additional myosin binding site. These data are consistent with an HSP70/HSP90 independent role of the TPR domain in yielding functional myosin[29]. Class-II crosslinks with myosin map to an N-terminal region (residues 30-150) adjacent to the SH3-like domain, residues 550-598 of the lower 50 kDa subdomain and the C-terminal part of the myosin motor adjacent to the converter region **(Fig. 1d)**. Importantly, most interlinks are located on the same face of the myosin molecule, extending from the actin-binding site to the SH3-domain **(Fig. 1e)**. The defined crosslinking pattern between UNC-45 and MHC-B suggests that the two proteins bind to each other in a structurally defined manner as expected for folded proteins. Contrary, in the UNC-45:myo^{UF} complex, UNC-45 is engaged in many unspecific interlinks with myosin (**Fig. 1d)**. When plotting these interlinks, the unfolded nature of myosin is reflected by continuous streaks of dots **(Supp, Fig. 2)**, suggesting that the relevant residues are part of disordered segments that arbitrarily interact with nearby sites. Moreover, the contacts are not restricted to clearly defined regions of myosin but rather involve all subdomains. In conclusion, the comparative SEC and XLMS analysis indicate that UNC-45 is capable of binding its substrate in folded and unfolded conformations, yielding functionally different chaperone:substrate complexes.

The folding state of myosin determines its interactions with PQC factors

To investigate whether the folding state of the captured substrate influences the channeling into folding and degradation pathways, we tested how the UNC-45:myo complexes interact with the molecular chaperone HSP90 and the UFD-2 ubiquitin ligase, respectively. Owing to the binding of HSP90 to the UNC-45 TPR domain[29], we performed interaction assays with the K82E mutant of UNC-45. As this mutant is known to abrogate TPR-dependent binding[13], it allows to selectively monitor the interaction of HSP90 chaperone with the captured myosin. Upon co-expression in insect cells, UNC-45^{K82E}:myo complexes isolated by tandem affinity chromatography showed a similar SEC profile as the complexes with wildtype UNC-45, being engaged with myo^{F} and myo^{UF} **(Fig. 2a)**. In pull-down assays, HSP90 bound to both

UNC-45^{K82E} complexes containing either intact or unfolded myosin (**Fig. 2a)**. This finding is consistent with HSP90 playing a dual role in maintaining the functionality of already folded and assembled myosin molecules in muscle sarcomeres[21] as well as serving as an E3 ligase co-factor in protein degradation pathways.

We next addressed the interplay between UNC-45, myosin and UFD-2, the ubiquitin ligase implicated in myosin quality control[20]. To map interaction sites between substrate, adaptor and E3 ligase, we pursued an XLMS approach. The three proteins were mixed in stoichiometric amounts and incubated at 4°C or 27°C, with the higher temperature selectively destabilizing myosin. Only when incubated at 27°C, a functional complex between UNC-45, myo^{UF} and UFD-2 was formed (**Fig. 2b**), Recently it has been proposed that UFD-2 can interact with the TPR domain of CHN-1 and stimulate its E3 ligase activity through an internal EEYD motif near the catalytic Ubox domain[30] (**Supp Fig. 3b**). Our XLMS data of the UFD-2/UNC-45/myosin complex indicates that UFD-2 also interacts with the UNC-45 TPR domain, however rather through an uncharacterized motif in the center of the ubiquitin ligase (residues 271-322, **Fig. 2c**, **Supp. Fig. 3b**), pointing to a different binding mode. Interestingly, UFD-2 engages the myosin substrate in a specific manner, as evidenced by crosslinks between its catalytic Ubox module and the terminal segments of the myosin motor domain **(Fig. 2c)**. To test the functional relevance of the inter-crosslinks, we performed *in vitro* ubiquitination assays and mapped the ubiquitination sites on myosin. We observed that at higher temperature, when myosin is destabilized and complex formation is favored, the ubiquitination reaction was markedly enhanced (**Supp. Fig. 3a)**, confirming the selective targeting of misfolded myosin. Mapping the ubiquitination sites of myo^{UF} revealed that UFD-2 preferentially targets lysine residues in the N- and C-terminal regions of the motor domain, as predicted by the XLMS analysis **(Fig. 2d)**. We thus propose that the central portion of the myosin motor, recognized and bound by UNC-45, is present in a mostly unfolded conformation enabling the N- and C-terminal segments to access the Ubox of the E3 enzyme. To further evidence the preference of UFD-2 for targeting an unfolded substrate, we performed *in vitro* ubiquitination assays with natively purified chaperone:substrate complexes and assessed myosin ubiquitination over time **(Fig. 2e-f, Supp. Fig. 3c)**. As predicted, UFD-2 showed a clear preference for ubiquitinating myosin contained in the UNC-45:myo^{UF} complex, whereas the reaction was slower and less efficient for UNC-45:myo^{F}. In sum, our data show that UNC-45

can form distinct complexes with folded and unfolded myosin, which are then evaluated for structural integrity by the downstream acting ubiquitin ligase UFD-2, leading to selective ubiquitination of the aberrant client protein.

UNC-45 recognizes a distinct β-hairpin in the myosin motor domain

To better understand the structural requirements for UNC-45:myo complex formation, we analyzed whether UNC-45 recognizes a specific consensus motif. To this end, we synthesized a peptide library the motor domain of MHC-B and assayed the interaction with UNC-45. The longest stretch of consecutive peptides bound by UNC-45 comprised myosin residues 547-588 (**Fig. 3a**). To validate the interaction patch, we probed the membrane with two binding-deficient UNC-45 mutants, lacking either the entire UCS-domain (ΔUCS, lacking residues 522-914) or the UCS-loop implicated in myosin binding[13,31] (Δloop, lacking residues 602-630). For both ΔUCS and Δloop variants, we observed several non-specific hits, however, they did not bind to the 547-588 motif recognized by wildtype UNC-45 **(Fig. 3a)**. Notably, the 547-588 stretch corresponds to a β-hairpin in the motor domain that is engaged in most class-II interlinks with UNC-45 in the XLMS datasets (**Fig. 1d**, **Fig. 3b**).

To confirm that the identified myosin stretch mediates UNC-45 binding in a specific manner, we characterized this interaction by thermal shift assays. In this approach, the stability of a protein – reflected by the melting temperature T_m – is measured in the presence of ligands, assuming that ligand binding increases protein stability. To control for non-specific binding events, we used the UNC-45 ΔUCS mutant and a peptide with a randomly scrambled sequence of the myosin motif **(Fig. 3c, Supp. Fig. 4a)**. Upon addition of the 547-588 myosin peptide, the melting temperature increased by 5.5°C, pointing to a direct interaction with UNC-45. Consistently, the ΔUCS mutant was not stabilized by the myosin peptide. Likewise, the scrambled peptide failed to stabilize wildtype UNC-45 to the same extent of the myosin peptide. Fluorescence anisotropy measurements, which were carried out in a qualitative manner due to low affinity of the binder, confirmed the specific interaction between the identified myosin ligand and UNC-45 **(Supp. Fig. 4b)**. In sum, these data indicate that residues 547-588 of the myosin motor domain contain the primary interaction site for UNC-45.

Structure of minimal UNC-45:myosin complex reveals FX_3HY motif

To investigate the structural basis of myosin recognition, we pursued a crystallographic approach. Given the difficulties in obtaining a co-crystal structure with *C. elegans* UNC-45, we moved to the less complex fungal orthologue SHE4. Despite lacking the TPR-domain, SHE4 contains a functional UCS-domain for myosin binding[13,32]. Moreover, sequence alignments indicated that the myosin motif recognized by UNC-45 is conserved in fungal isoforms **(Fig. 4a)** and has been previously postulated to be part of the SHE4 binding motif[32]. Bioinformatic analysis revealed that *Kluyveromyces lactis* SHE4 is the most promising candidate for crystallographic studies, having a functional UCS domain but lacking various flexible, non-conserved regions that impeded crystallization of the yeast ortholog[32] **(Supp. Fig. 5a)**. In fact, the 76 kDa protein readily crystallized, enabling us to determine the structure of wildtype $SHE4_{KL}$ at 2.4 Å resolution **(Supp. Fig. 5b)**. Overall, $SHE4_{KL}$ resembles an L-shaped superhelix that is composed of a short, flattened N-terminal arm and an extended, slightly bent UCS-domain that aligns well with the UCS-domain of *C. elegans* UNC-45 (root mean square deviation: 3.8 Å for 321 Cα-atoms) **(Supp Fig. 5b)**. Both fungal and metazoan UCS-domains are composed of a series of Armadillo repeat motifs (ARM), each of which is defined by a short helix (H1) followed by two elongated helices (H2, H3) that stack in a perpendicular manner **(Supp Fig. 5b)**. In the resulting superhelical UCS-scaffold, the ARM-repeat H3 helices line the concave face of the substrate-binding canyon to mediate interactions with myosin[33].

To characterize the structural motif recognized by the UCS domain, we synthesized a series of Myo4 peptides, encompassing the β-hairpin motif 547-588 identified in the peptide spot assay. Isothermal titration calorimetry (ITC) measurements showed that 13 residues (561-573) comprise the core of the myosin motif, binding to $SHE4_{KL}$ with a K_D of 0.6 µM **(Fig. 4b)**. After intense co-crystallization trials with various myosin peptides, we obtained a well-diffracting SHE4 co-crystal with a peptide comprising Myo4 residues 561-581. We determined the co-crystal structure at a resolution of 2.4 Å and were able to visualize a minimal SHE4:Myo4 complex in atomic detail. In this structure, the Myo4 residues Lys561-Phe562-Ile563-Val564-Ser565-His566-Tyr567 were well-defined by electron density **(Fig. 4e)**. The eight myosin residues are accommodated in the UCS-canyon by a dense network of hydrogen bonds and hydrophobic interactions. The tight binding mode forces the Myo4 peptide to adopt a

bent conformation, with its C-terminal portion being directed out of the central groove of the UCS-domain. Notably, this bent conformation is distinct from the β-turn observed in the native myosin structure, preventing UNC-45 to target functional myosin **(Supp. Fig. 6)**. As for its substrate, the interacting residues in the UCS domain of SHE4 are conserved across species **(Supp. Fig. 7)** suggesting that the observed binding mode is generally relevant. To validate the structural data, we mutated the strictly conserved Asn475 that is located in the UCS binding groove and binds to the backbone of the captured myosin peptide **(Fig. 4e, Supp. Fig. 7)**. ITC-measurements showed that binding to the myosin peptide was abrogated in the N475A mutant, confirming its participation in substrate binding **(Fig. 4c)**.

Given the conservation of the myosin residue Phe577, His581 and Tyr582, which are accommodated in specific pockets of the UCS canyon (**Fig. 4a-d**), we tested the general relevance of these residues in the *C. elegans* system. Since UNC-45 precipitated during ITC measurements, we performed thermal shift measurements, incubating UNC-45 with the respective MHC-B peptide. Contrary to the native peptide that elevated UNC-45 stability by 5.5°C, introducing the F577A, H581A or Y582A mutations only resulted in a minor increase in T_m **(Supp. Fig. 8a**). Consistently, fluorescence anisotropy measurements supported the crucial role of these residues in mediating UNC-45 binding, as F577A, H581A and Y582A myosin peptides were strongly impaired in their interaction with UNC-45 (**Fig. 5a**). Furthermore, the binding of this motif to UNC-45 fits well to our crosslinking data (**Fig. 1d**), according to which myosin residues 576-587 are accommodated in the center of the UCS canyon, juxtaposing the adjacent motor domain regions to the UNC-45 chaperone. The observed crosslinks suggest that the complex is held together on one side by links from myosin residues Lys550 and Lys558, and on the other side by a link from residue Tyr588 (**Fig. 3b**). In concert, these interactions yield a chaperone-substrate complex with a well-defined topology that locks the β-hairpin motif in place. Taken together, our structural and biochemical data indicate that the conserved myosin residues Phe577, His581 and Tyr582 mediate binding to *C. elegans* UNC-45. We thus propose that the respective FX_3HY motif represents a universal and highly specific substrate epitope, recognized by the myosin-specific chaperone UNC-45.

Disruption of the FX_3HY motif abolishes myosin folding in the cell

To test the functional relevance of the FX_3HY-motif in a cellular context we monitored UNC-45 dependent maturation of myosin in insect cells[29]. Since UNC-45 is essential to produce soluble myosin, UNC-45/myosin co-expression can be used as a proxy for evaluating chaperone-substrate interactions. By assessing the yields of soluble myosin produced in insect cells, we found that replacing the β-hairpin loop (581-HYAG-584) with a GSGS spacer impairs UNC-45-dependent myosin folding **(Fig. 5b)**. Strikingly, the same deleterious effect was observed for the single-site mutants F577A, H581A or Y582A **(Fig. 5b-c)**, highlighting the impact of the FX_3HY motif on myosin maturation. We then looked for disease causing mutations in this motif and found that the Freeman-Sheldon Syndrome (FSS), a myopathy associated with severe multiple congenital contracture[34], is linked to the substitution of a serine at the conserved Tyr582 site. To explore whether the Y582S mutation may impact interaction with UNC-45, we co-expressed the respective MHC-B variant with UNC-45 in insect cells and observed that this mutation significantly decreased the levels of soluble myosin **(Fig. 5c)**. Fluorescence anisotropy measurements with a myosin peptide carrying the Y582S mutation confirmed the in vivo data, as binding to UNC-45 was markedly reduced **(Fig. 5a)**. The resultant misfolding of myosin may underlie the phenotype observed in a *Drosophila melanogaster* FSS disease model, in which the Y582S mutation led to a progressive disruption of muscle sarcomeres, although the kinetic properties of the isolated mutant were more similar to wildtype myosin when compared to other FSS mutants[27]. Contrary to the Y582S mutation, introducing a Y582F mutation had milder effects. In fluorescence anisotropy experiments, the Y582F mutant showed slightly lower UNC-45 affinity compared to the native peptide **(Fig. 5a)**, while in the cellular chaperone assay, the amounts of soluble myosin were comparable to that of wildtype protein **(Fig. 5c)**. Consistently, *C. elegans* non-muscle myosins contain a Phe582, suggesting that the phenyl ring at this position is sufficient for UNC-45 assisted folding (**Supp. Fig 8b**). Taken together, our *in vitro* and *in vivo* data highlight the importance of the conserved FX_3HY motif to mediate interactions with UNC-45 and promote myosin folding. Moreover, our findings directly connect the Y582S mutation found in FSS myopathy to myosin quality control, preventing chaperone binding thus interfering with myosin maturation and causing aggregation of the muscle protein.

Discussion

Structural characterization of chaperone-substrate interactions is challenging due to the heterogeneity of respective complexes, which contains a continuum of transient folding intermediates. Advances in cryo-electron microscopy and NMR spectroscopy allowed visualization of certain chaperone-substrate complexes[26,35–43], delineating the targeting mechanisms of general chaperones including HSP90, HSP70 and TriC[26,35–43]. Conversely, the mode of action of the many client-specific folding factors is less understood, with notable exceptions being the histone and Rubisco chaperones[44,45]. To better understand substrate targeting by specialized chaperones, we studied the interplay between UNC-45 and its client protein myosin. By applying an integrative structural biology approach, we show that the highly conserved FX_3HY motif present in the myosin motor domain is a discrete molecular epitope recognized by the UNC-45 chaperone, which then presents the bound client to downstream PQC factors.

An important feature of the PQC decision-making process is that UNC-45 can accommodate both folded and misfolded myosin. Upon forming separate complexes with the two myosin forms, downstream acting chaperones and E3 ligases channel the presented client into folding or degradation pathways **(Fig. 6)**. Whereas the general chaperones, as shown here for HSP90, seem to obtain an indirect role preventing premature myosin aggregation and keeping the (partially) misfolded protein in solution, the UFD-2 ubiquitin ligase takes the decision. Only the severely damaged myosin is targeted whereas folded myosin in complex with UNC-45 is channeled into assembly pathways. Importantly, for myosin ubiquitination by UFD-2, formation of a productive E3 ubiquitin ligase complex depends on a composite signal, provided by the UNC-45 adaptor (available TPR docking site, not occupied by HSP70/HSP90 chaperones) and the captured myosin (misfolded state). The proposed model thus exemplifies how different components of the cellular PQC system collaborate and compete with each other to decide in concert about the fate of a given substrate protein, i.e. folding vs. degradation.

The stable complex of UNC-45:myo^F with predominantly folded myosin implies that UNC-45 not only mediates the initial stages of protein folding, but also possesses a function beyond, a finding that is compatible with the role of UNC-45 in thick filament assembly and stress response[13,21]. Chaperone complexes, which engage with folded substrates, have also been observed in other biological pathways. For example, a

specific J-domain protein was shown to bind natively folded tau in order to prevent protein aggregation[46]. Intriguingly, Tyr582 of the myosin FX_3HY-motif has to fulfill two critical functions. First, Tyr582 has been shown to promote structural rearrangements in the myosin motor required for the ATP-driven power stroke[47,48]. In addition, as shown here, Tyr582 is one of three conserved myosin residues that is essential for UNC-45 binding. Given the importance of Tyr582 for motor activity and myosin folding, our findings suggest that binding of UNC-45 to myosin could have a regulatory role, coupling chaperone engagement with inhibition of ATPase activity. This regulation might be critical to keep the myosin motor in a resting state during protein folding, sarcomere assembly or under stress conditions. Consistently, a previous study highlighted the role of UNC-45 in inhibiting the myosin power stroke, and suggested that inhibition is achieved through interactions with the UCS domain[49]. The respective interplay between UNC-45 and myosin is now resolved in molecular detail, revealing a highly specific binding mode tailored to target a key functional motif of the client. Other client-specific chaperones are likely to also target conserved functional sites in their substrates, ensuring a high selective pressure to maintain specialized folding pathways.

Myosin-linked myopathies have been mostly studied in the light of deregulated myosin ATPase activity that impairs the actomyosin cross-bridge cycle[50] or the energy-saving super-relaxed state (SRX)[51,52]. Interestingly, mutations in chaperones like Bag3[53] and DnaJB6[54] cause congenital muscle defects, and HSPB6, HSP70 and HSP90 are upregulated upon cardiac failure[55,56], pointing to the importance of an efficient PQC system to prevent myosin-related myopathies. Consistently, human UNC-45B mutations have been linked to mild forms of myopathy, attributed to reduced stability of the chaperone itself[17]. The characterized mutations are localized in the UCS domain, close to residues identified as myosin interaction sites **(Supp. Fig. 9)**, suggesting that they might impact not only UNC-45 stability, but also substrate interactions. We thus propose that myosin proteostasis, and specifically UNC-45:myosin interactions, play an important yet underestimated role in myopathies. The importance of a functional PQC system for preventing human myopathies is reflected by the Y582S mutation in the FX_3HY motif, underlying FSS developmental myopathy[34]. This point mutation abolishes the interaction with UNC-45, leading to myosin misfolding and aggregation. To our knowledge, these findings provide the first direct link between impaired myosin quality control and the onset of

myopathies, offering new paths for medical intervention. Moreover, our data indicate that disease causing mutations in myosin and UNC-45 are recapitulated by the *C. elegans* proteins. Given its powerful genetics and emerging role to study protein misfolded diseases[57–59], *C. elegans* should be an attractive model system to delineate cellular pathways causing myosin-based myopathies and explore counteractive strategies.

Acknowledgements

We thank all members of the Clausen lab for critical remarks on the manuscript. Furthermore, we are grateful to the staff at DESY (Hamburg, Germany) and ESRF (Grenoble, France), where the diffraction data were recorded. We would also like to thank the VBCF Mass Spectrometry Facility in particular Elisabeth Roitinger and Karl Mechtler for their assistance as well as the VBCF Protein Technologies and Anita Lehner for helping with protein production. Moreover, we are grateful to Mathias Madalinski for synthesizing the peptides.. AV was supported by the DOC fellowship from the Austrian Academy of Sciences (ÖAW). The IMP is supported by Boehringer Ingelheim.

Autor contributions

Conceptualization, A.V., R.A. and T.C.; Methodology, A.V. and R.A.; Investigation A.V, R.A. and R.M.G.C.; Resources, D.S., A.L. and A.B.; Writing – original draft, A.V., R.A. and T.C.; Writing - Review and editing, R.A. and T.C.; Visualization, A.V. and R.A.; Supervision, A.M and T.C; Funding Acquisition, A.V. and T.C.

Declaration of interests

The authors declare no competing interests.

Figures and Figure Legends

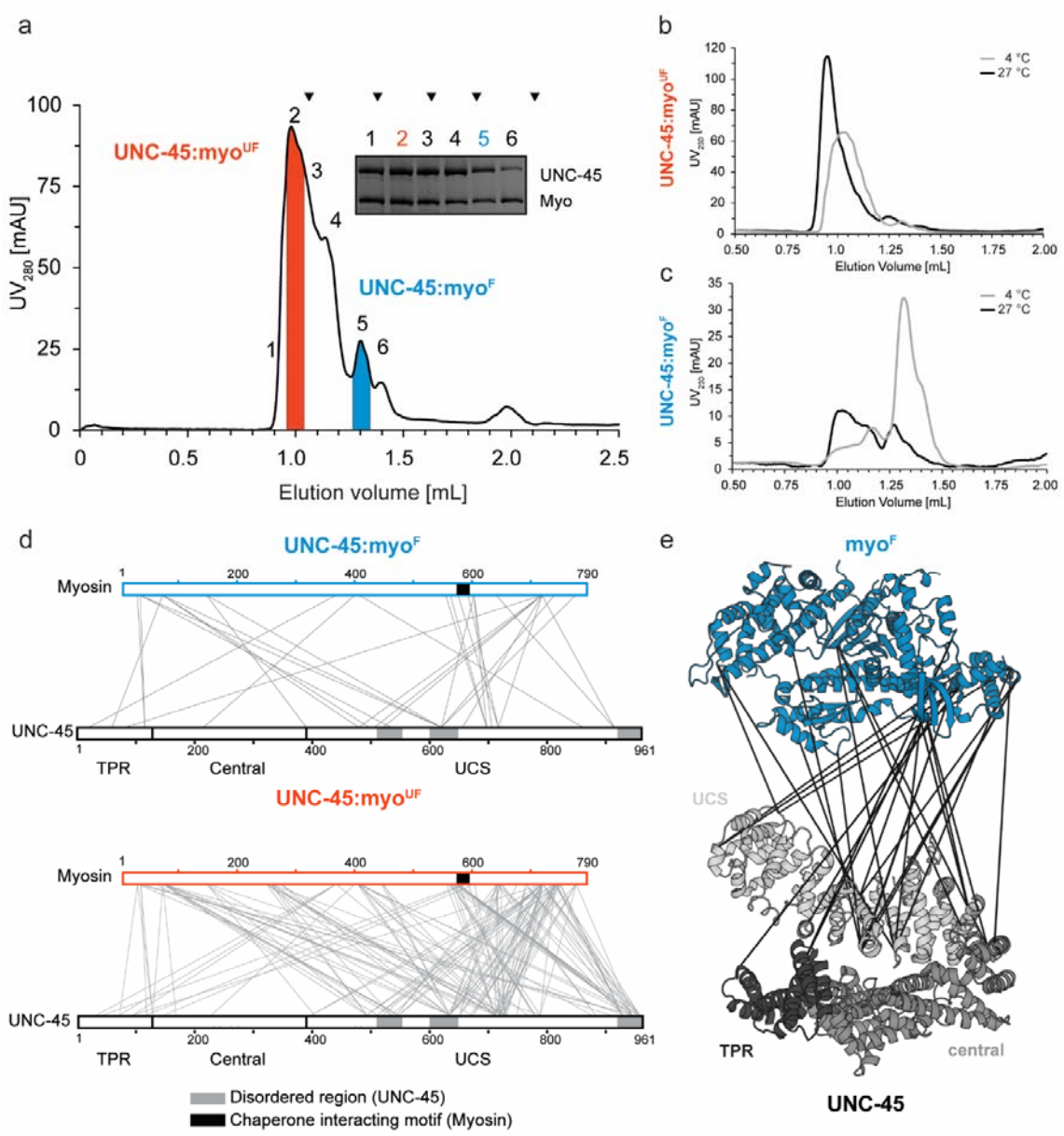

Figure 1: UNC-45 can form distinct complexes with folded and unfolded myosin

(a) UNC-45:myosin complex purification, involving tandem-affinity chromatography and SEC. In the final SEC run, UNC-45 complexes with folded (myo^{F}) and unfolded (myo^{UF}) myosin can be separated. As seen in SDS-PAGE, chaperone and substrate associate in stoichiometric manner. For follow-up experiments, only the red (UNC-45:myo^{UF}) and blue (UNC-45:myo^{F}) coloured fractions were used. Molecular markers are indicated by arrowheads (670 kDa, 158 kDa, 44 kDa, 17 kDa, 1.35 kDa). **(b-c)** SEC analysis of UNC-45:myosin complexes incubated at 4°C (grey) and 27°C

(black), with the higher temperature selectively destabilizing folded myosin. **(d)** XLMS analysis of UNC-45:myosin complexes, showing interlinks with myo^{F} (top) and myo^{UF} (bottom). Illustrated crosslinks here and in the following figures have been filtered to FDR ≤ 5%. **(e)** Interlinks of the UNC-45:myo^{F} complex are mapped on the crystal structures of UNC-45 (PDB: 4i2z, grey) and myosin (PDB: 6qdj, blue), highlighting the clearly defined arrangement of the two proteins .

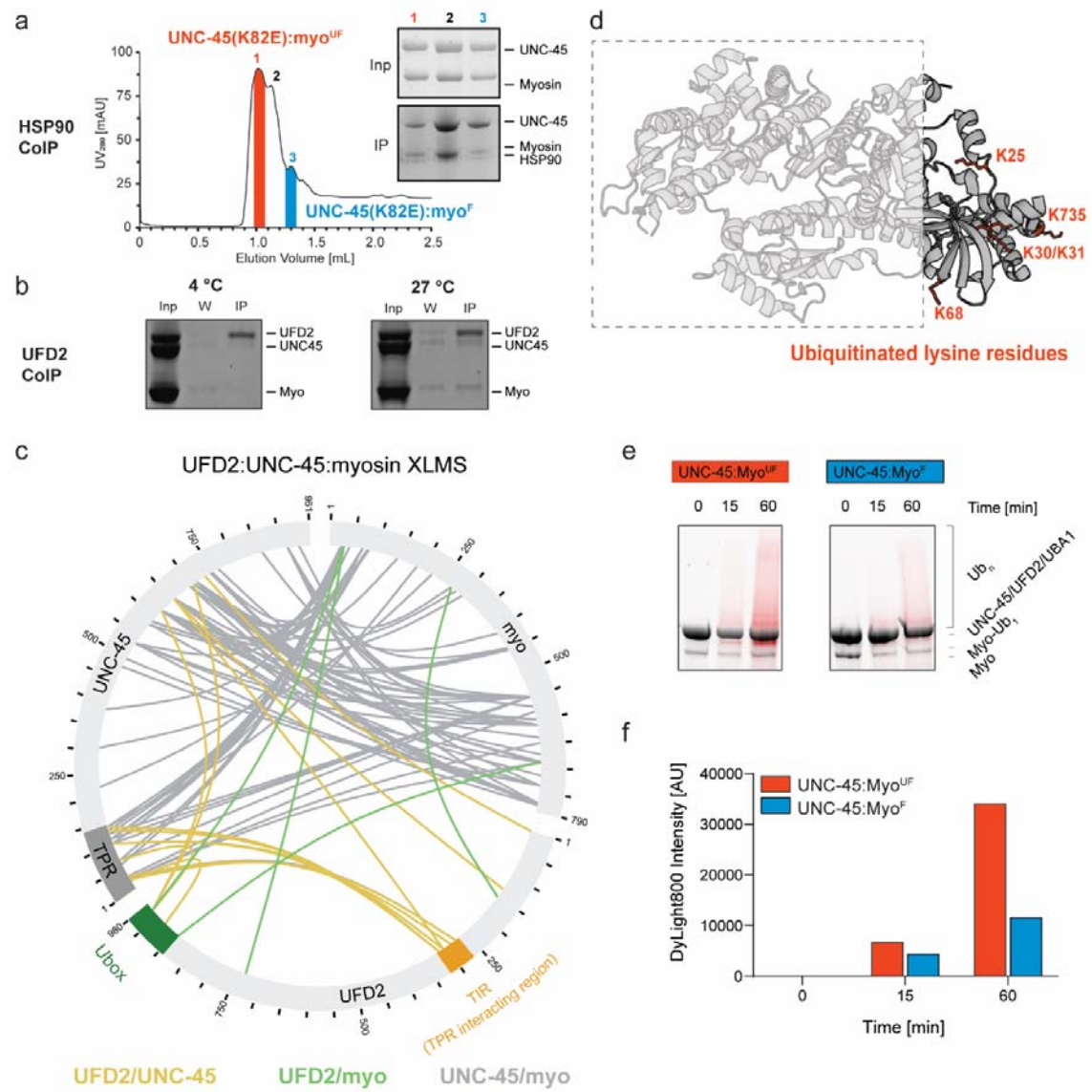

Figure 2: PQC factors interact in a specific manner with UNC-45:myo^{F} and UNC-45:myo^{UF} complexes

(a) Purification of UNC-45(K82E):myo complexes and pull-down with HSP90 probing TPR-independent interactions with recombinant HSP90, reveals binding to both myo^{UF} and myo^{F}. **(b)** Pull-down assay with UFD-2 reveals selective binding to UNC-45:myosin at elevated temperature (27°C) when myosin becomes unfolded. **(c)** XLMS analysis of in vitro reconstituted UFD-2:UNC-45:myo^{UF} complex. Crosslinks between UFD-2/UNC-45 are coloured blue; between UFD-2/myo^{UF} red and between UNC-45/myo^{UF} grey. **(d)** Mapping of UFD-2 mediated ubiquitination sites on myo^{UF}. Identified sites cluster in N- and C-terminal myosin segments near the identified crosslinks to the catalytic Ubox domain of UFD-2. **(e)** UFD-2 mediated ubiquitination of natively purified UNC-45:myosin complexes containing the folded and unfolded

substrate, respectively. In the SDS-PAGE gels, the stain-free fluorescence (total protein) and DyLight800 (ubiquitin) signals are overlaid. **(f)** Quantification of the poly-ubiquitination of myo^{UF} and myo^{F} presented by UNC-45 to UFD-2, showing increased activity with myo^{UF} as a substrate.

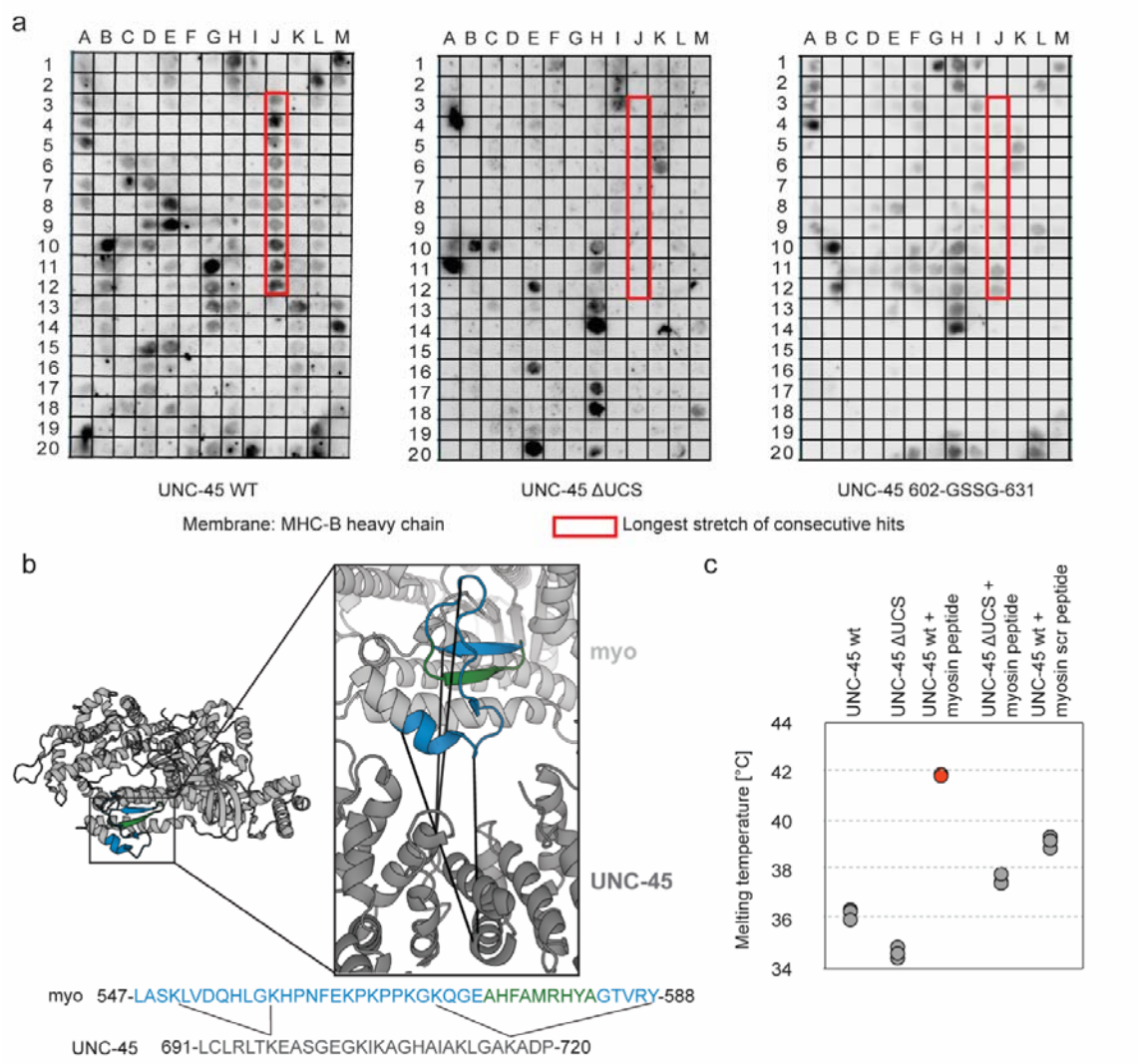

Figure 3: UNC-45 recognizes a concise motif in the myosin motor domain

(a) Peptide spot analysis (MHC-B peptides of 15-residue per spot, with 12 residue overlap) of UNC-45 binding to myosin. ΔUCS and Δloop variants were used as binding-deficient controls. The longest stretch of consecutive hits is highlighted with a red box. **(b)** Mapping of the binding epitope on MHC-B myosin crystal structure (PDB: 6qdj). The inset highlights the consistency of the peptide spot data (highlighted in blue) with the XLMS data (specific crosslinks undergone between myosin and UCS domain of UNC-45). The corresponding protein sequences are indicated below, together with the crosslinked residue and the later on identified minimal binding motif (green). **(c)** Thermal shift assays addressing the binding of the identified motif to UNC-45. The ΔUCS chaperone and a scrambled (scr) myosin peptide were used as control. Assays have been performed in triplicates.

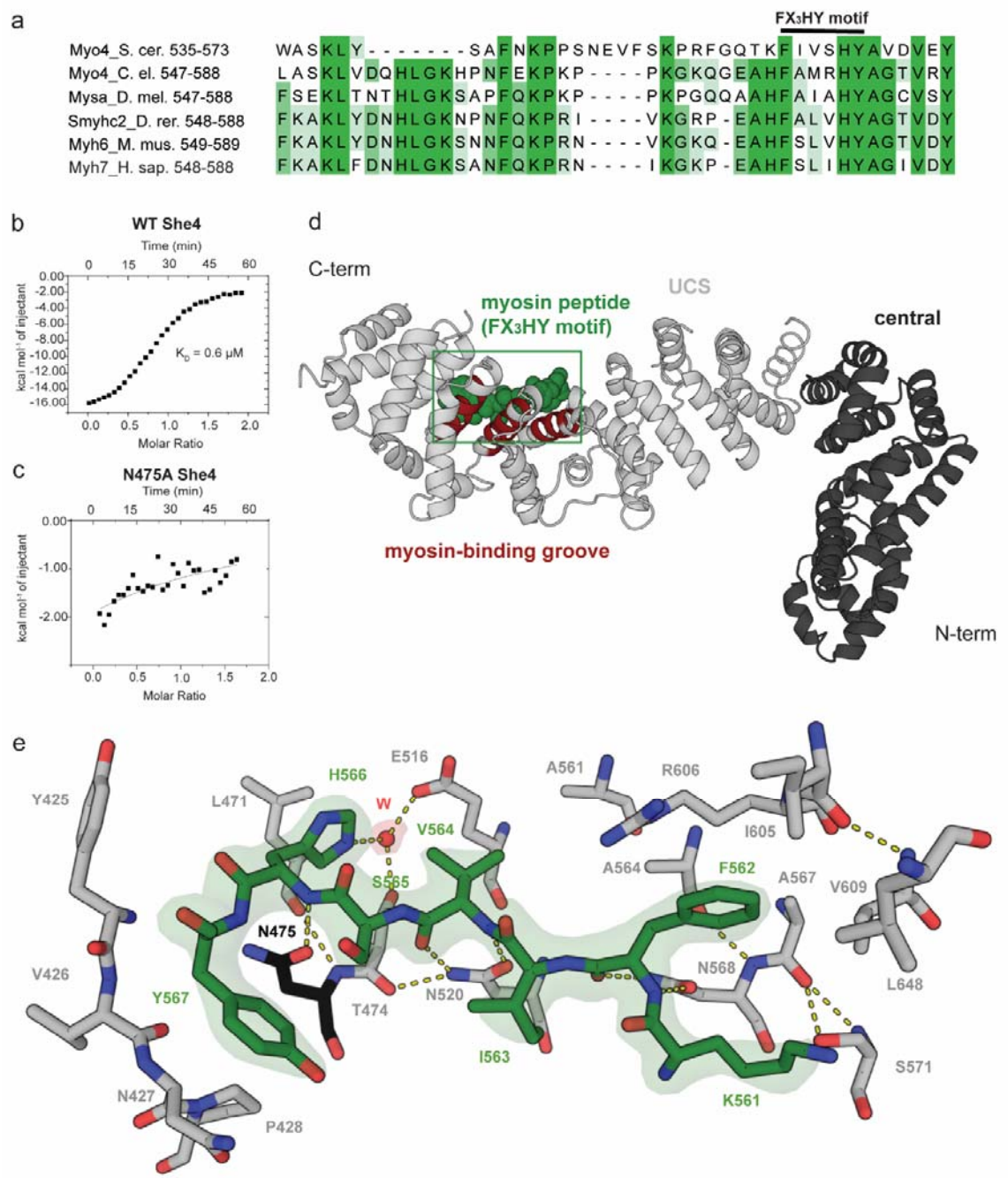

Figure 4. Crystal structure of a minimal UNC-45:myosin complex

(a) Sequence alignment of the identified UNC-45 interaction motif in MHC-B (Myo4_Cel). Residues are colored according to sequence identity (dark blue >80%, white <40%). Conserved residues that define the FX_3HY motif are labelled. **(b)** ITC measurement of Myo4 peptide (residues 561-573) binding to SHE4, the yeast ortholog of UNC-45. **(c)** As in **(b)** with N475A SHE4, a mutation in the UCS canyon that abolishes myosin binding. **(d)** Co-crystal structure of the minimal SHE4:Myo4 complex, highlighting the bound myosin peptide defined by the electron density

(residues 561-567, green) and the central part of the myosin binding groove (brown). UCS and central domain are depicted in gray and black, respectively. **(e)** Detailed view on SHE4:Myo4 interactions, with key residues being labelled and selected hydrogen bonds shown in yellow and a coordinating water molecule in red. Asn475 mutated to Ala in functional assays is colored in black. The 2Fo-Fc electron density of the peptide is contoured at 1.5 σ and shown as surface representation.

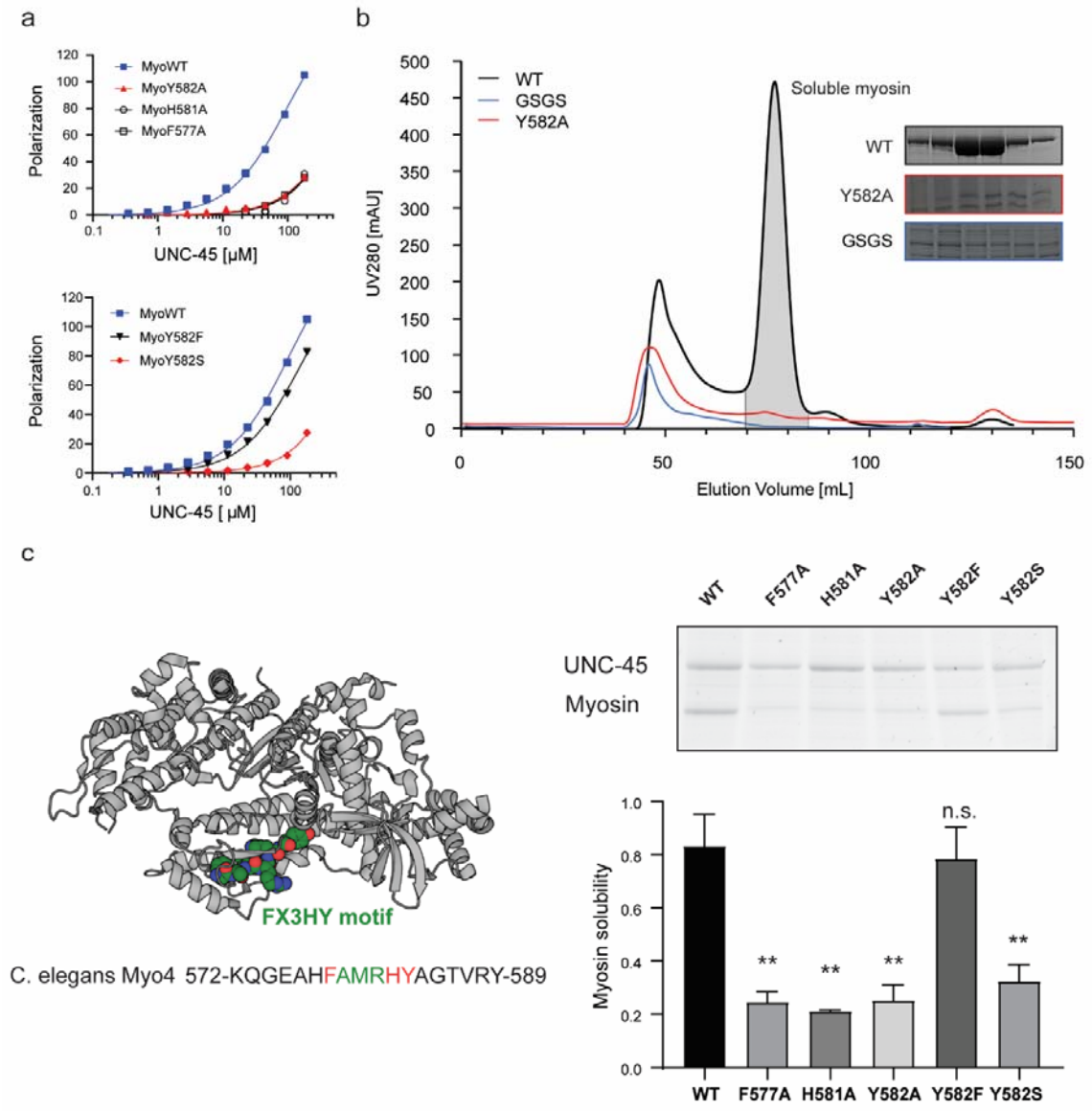

Figure 5 The FX_3HY-motif is essential for UNC-45 binding and myosin folding

(a) Fluorescence polarization experiments comparing a wildtype myosin peptide with mutants of the conserved FX_3HY-motif. Increasing concentrations of purified UNC-45 were titrated to fluoresceine labelled peptides. **(b)** SEC analysis of purified myosin motor domain comparing wildtype, Y582A (red) and R580-GSGS-T585 (blue) variants. Fractions eluting at the size of the functional motor domain (~75 ml, grey peak) were analyzed by SDS-PAGE. **(c)** In cell solubility assay of myosin variants containing mutations in the FX_3HY-motif. Cleared insect cell lysates were analyzed by SDS-PAGE and the relative amount of soluble myosin quantified by comparing protein levels to UNC-45. Mean and SD of 3 biological replicates are shown. Two

asterisks denote statistical significances (t-test p-value<0.01) and n.s. denotes no statistical significance compared to wildtype.

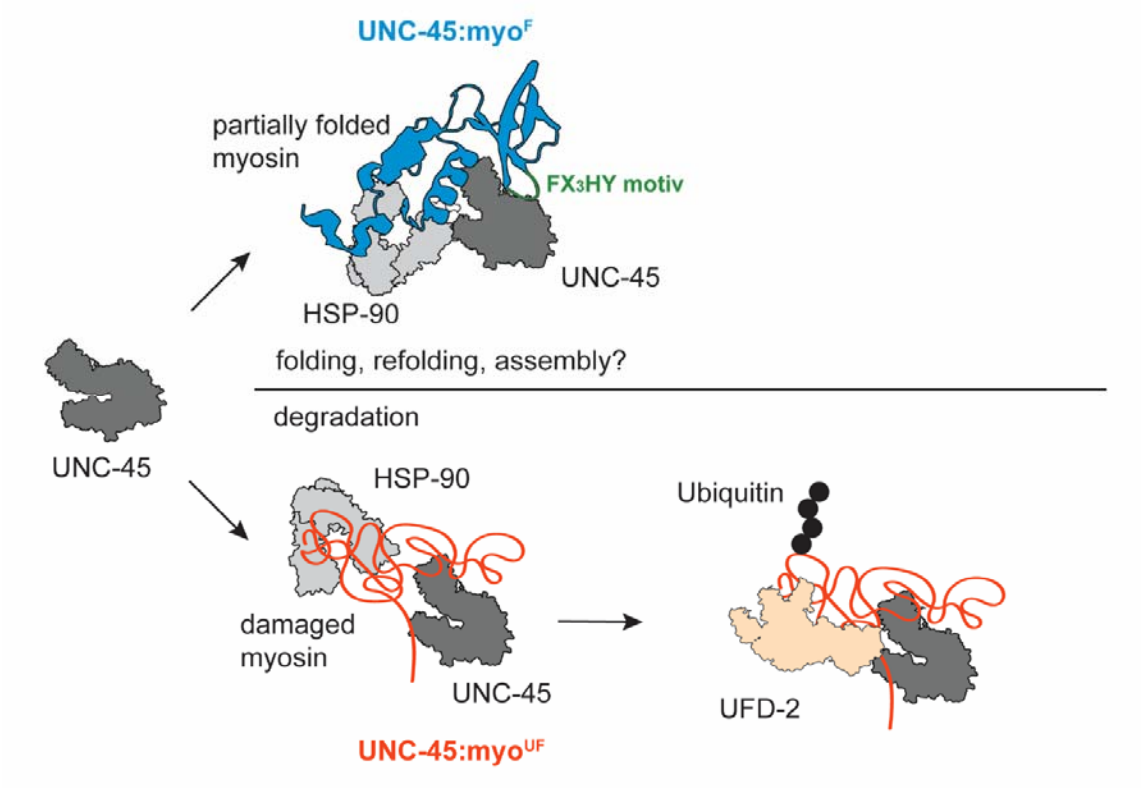

Fig. 6 Model of the interplay of UNC-45 with partner PQC factors to determine the fate of its myosin client

UNC-45 can bind to myosin present in different conformations (folded or unfolded; recognized by the FX_3HY motif) and channel it into folding or degradation pathways. In the UNC-45:myo^F complex shown in the top panel, the myosin motor domain exists in a close to native conformation (blue), as expected for a late folding intermediate prior to incorporation into thick filaments or resulting from mild proteotoxic stress. HSP90 (grey) is involved in this assembly pathway as well. Contrary, irreversibly damaged myosin (orange) captured in the UNC-45:myo^{UF} complex is channelled by UNC-45 and its partner chaperones HSP70/HSP90 (grey) to the quality-control ubiquitin ligase UFD-2 (light orange), inducing its poly-ubiquitination and proteasomal degradation.

Methods

Protein production and purification from *E. coli*

SHE4 was amplified from *Kluyveromyces lactis* cDNA and cloned into a pET21a vector to generate the C-terminally His_6-tagged protein. The protein was expressed in BL21(DE3) cells which were induced with 100 µM IPTG and incubated at 18 °C overnight. Cells were harvested by centrifugation, resuspended in 50 mM Tris pH 7.2, 300 mM NaCl, 1 mM TCEP (Buffer A) and lysed by sonication. The cleared lysate was applied to a Ni-NTA Superflow column (Qiagen). The column was washed with buffer A and a high salt buffer containing 50 mM Tris pH 7.2, 1 M NaCl, 1 mM TCEP. SHE4-elution was performed with buffer A containing 60 mM imidazole. The elution fraction was loaded on a Bio-Gel HT Hydroxyapatite column (Bio-Rad) equilibrated with buffer A, and the protein was eluted in a linear gradient until 100 mM KH_2PO_4. For the final step of purification, SHE4 was subjected to size-exclusion chromatography using a Superdex 200 16/60 column (GE Healthcare) equilibrated with 10 mM Tris pH 7.2, 300 mM NaCl, 1 mM TCEP (for crystallization trials) respectively 10 mM HEPES pH 8.0, 150 mM NaCl, 1 mM TCEP (for ITC).

Full length UNC-45 and UNC-45ΔUCS proteins were expressed and purified as previously described[13]. In short, expression was induced with 100 µM IPTG for 12 hours at 18 °C. Cells were harvested by centrifugation and lysed by sonication in 50 mM NaH_2PO_4 pH 8.0, 300 mM NaCl (His-tag) or 100 mM Tris pH 8.0, 150 mM NaCl, 1 mM EDTA (Strep-tag). Tagged proteins were purified by affinity chromatography (HisTrap resp. StrepTrap, both GE Healthcare) with elution buffer containing 200 mM imidazole respectively 2.5 mM d-desthiobiotin. Proteins were then subjected to size-exclusion chromatography using a Superdex 200 16/60 column (GE Healthcare) equilibrated with 20 mM HEPES, pH 8.0, 150 mM NaCl. For ubiquitination assays UBA1 (*H. sapiens*), LET-70 and UFD-2 (both *C. elegans*) were purified as described previously[20].

Protein production and purification from insect cells

The *C. elegans* myosin motor domain MHC (1-790) wildtype and mutants (F577A, H581A, Y582A, Y582F, Y582S, R580-GSGS-T585) were expressed as described previously[29]. MHC-B (*C. elegans*) containing a C-terminal His_6-tag was cloned into the polyhedrin promotor site of the pFastBac DUAL vector (Invitrogen). Baculoviruses

for respective constructs were produced by transfecting Sf9-cells (Expression Systems) with FuGENE HD (Promega). For protein expression, High Five cells (Expression Systems) in suspension culture at a density of $1x10^6$ cells/ml were infected with baculovirus (V1) and incubated at 21 °C for 96 hours.

For myosin purification cell pellets were resuspended in 50 mM Tris pH 8.0, 300 mM NaCl (buffer A), 1:10 000 benzonase was added and cells were lysed with a homogenizer. The cleared lysate was loaded onto a NiNTA column (GE Healthcare) equilibrated with buffer A. The column was washed with buffer A, and myosin was eluted with buffer A, containing 200 mM imidazole. The elution fractions were applied to a Superdex 200 16/60 column (GE Healthcare) equilibrated with 20 mM HEPES pH 8.0, 150 mM NaCl. For purification of UNC-45-myosin complexes, the fractions eluting from the HisTrap column containing myosin were loaded on a Strep-Tactin gravity flow column (IBA Lifesciences) equilibrated with 100 mM Tris pH 8.0, 150 mM NaCl, 1 mM EDTA (Strep buffer A). The UNC-45-myosin complex was eluted with buffer A containing 2.5 mM d-desthiobiotin. To separate the different complex fractions, the sample was loaded onto a Superdex 200 3.2/300 column (GE Healthcare) equilibrated with 20 mM HEPES pH 8.0, 150 mM NaCl.

Isothermal titration calorimetry (ITC)

For peptide quantification a tryptophan was introduced at the N-terminus. This residue is visible in the SHE4-myosin co-crystal structure but was omitted from the discussion since it is not part of the native protein sequence. ITC for characterizing interactions between SHE4 and the synthesized myosin peptides was performed at 25 °C with a VP-ITC (Microcal). Peptides and protein were diluted in 10 mM HEPES pH 8.0, 150 mM NaCl, 1 mM TCEP. For wildtype SHE4, the temperature-controlled sample cell was loaded with 10 µM protein solution and titrated with 90 µM ligand in the mixing syringe (SHE4 N475A: 10 µM SHE4 in the cell, 107 µM myosin peptide in the syringe). An initial injection of 5 µl was followed by 29 consecutive injections of 10 µl with 300 s equilibration time in between. Control experiments with buffer and peptide were performed to correct for the heat of dilution. Data were analyzed with the MicroCal Origin software using a single side binding model. The peptides were synthesized in-house on a Syro Peptide Synthesizer (Multisyntech) and HPLC purified.

Crystallization of SHE4 and SHE4-myosin peptide

SHE4-crystals were grown by sitting-drop vapor diffusion at 4 °C in 96-well plates. 100 nl protein solution (145.2 µM) was mixed with 100 nl reservoir solution (0.1 M HEPES pH 6.9, 10% PEG 8000, 30% ethylene glycol, 51.4 mM $CaCl_2$) and yielded crystals after 3 days. The conditions used for co-crystallization of SHE4 with the myosin peptide were 10% PEG 20000, 20% PEG MME 550, 0.03 M $MgCl_2$, 0.03 M $CaCl_2$, 0.1 M bicine/Trizma base pH 8.5.

The unit cell parameters of the $P3_121$ space group were 129.5 Å, 129.5 Å, 77.2 Å (SHE4) respectively $P3_121$ and 128.5 Å, 128.5 Å, 77.5 Å for SHE4 with the myosin peptide. C diffraction data of SHE4 were collected at the Deutsches Elektronen-Synchrotron (DESY) and for SHE-myosin peptide at the European Synchrotron Radiation Facility (ESRF). The crystal structure of SHE was determined by molecular replacement using the *C. elegans* UCS-domain as a search model (PDB: 4i2z). The initial model from Phaser[61] was submitted to rigid body and B-factor refinement in CNS[62] and yielded an improved electron density map. The initial model was built with O[63] and refinement of the final structure was performed with PHENIX.Ramachandran statistics were calculated with PHENIX. The apo-SHE4-structure was used for molecular replacement to help determine the crystal structure of SHE4 with the myosin peptide. For figure preparation PyMOL (Schrodinger) was used.

Protein sequence analysis

For conservation analysis of the UCS-domain representative proteins from the UNC-45, CRO1 and SHE4 family were selected. For analysis of myosin conservation, all annotated myosin sequences from the UniProt repository were used. Multiple sequence alignment was performed with MUSCLE[64] and conservation was plotted using Jalview[65] applying the BLOSUM62-score.

Peptide Spot assays

Myosin-peptides (MHC-B, *C. elegans,* residues 1-790) consisting of 15 amino acids were synthesized on a derivatized cellulose membrane (Intavis 32.100) using the ResPep SLi synthesizer (Intavis). The membrane was designed with an overlap of 12 amino acid residues compared to the neighboring peptide. The membrane was

activated with methanol, blocked with 3% bovine serum albumin (BSA) and incubated with 50 µg/ml Strep-tagged (C-term) wildtype UNC-45/UNC-45ΔUCS/UNC-45Δloop. The peptide spot membrane was blotted onto a nitrocellulose membrane and UNC-45 binding was probed with an anti-Strep antibody (Qiagen) using an ECL-kit for detection (GE Healthcare).

Thermal shift assays

These assays were performed in 96-well-plate format using a RT-PCR thermocycler (Biorad). 70 µl of wildtype UNC-45 or UNC-45 ΔUCS (1 µM), respective peptides (2 mM) and SYPRO Orange dye (5x) were prepared in 20 mM HEPES pH 8.0, 150 mM NaCl. For measurement, the plate was incubated at 12 °C for 3 minutes, then a gradient of 1 °C/min was applied up to 95 °C. Three samples for each combination of protein and peptide were measured.

Fluorescence anisotropy

Peptides (sequence AHRFAMHYA, and mutations indicated in the figures) were synthesized in-house, as described in a previous section, and contained a N-terminal fluorescein. Fluorescence anisotropy experiments were performed in a buffer containing 25 mM Tris pH 8.0, 150 mM NaCl. A peptide concentration of 2 µM was used. The starting concentration of UNC-45 was 180 µM which was subsequently diluted 1:1. Polarization was acquired with a PHERAstar microplate reader (BMG Labtech). Fitting was performed using a non-linear least squares algorithm in GraphPad Prism 8.

Ubiquitination assays

Ubiquitination assays were performed in 20 mM Tris pH 7.5, 50 mM NaCl, 1 mM DTT, 10 mM $MgCl_2$. The reaction mix contained 20 µM DyLight800-Maleimide-ubiquitin (prepared as described previously[66]), 0.5 µM E1 (UBA1), 1.2 µM E2 (LET-70), 1 µM E3 (UFD-2) and 10 mM ATP. To prepare the substrate for the assay containing *in vitro* reconstituted UNC-45:myosin-complex, equimolar ratios of both proteins were mixed and incubated at 4 °C or 27 °C for 60 minutes. 1.5 µM of this pre-incubated UNC-45:myosin was added to the ubiquitination assay reaction mix.

When purified UNC-45:myosin-complexes were used as substrate, 1 µM of the indicated SEC-fractions were subjected to the ubiquitination assay after purification without prior incubation. Ubiquitination assays were performed at 21 °C, at the respective timepoints the reaction was stopped by adding SDS-PAGE loading buffer and heating the sample to 95 °C for 5 minutes. Samples were electrophoretically separated on BioRad Stain-Free TGX 4–20% gels. Proteins modified with ubiquitin were visualized by DyLight800-fluorescence and total protein levels were measured using Stain-Free tryptophan fluorescence. Signals were quantified using Fiji software.

Analytical size-exclusion chromatography of UNC-45:myosin-complexes

SEC-fractions from UNC-45:myosin complex purification were split in half and incubated at 4 °C or 27 °C for 30 min. After incubation, samples were applied to a Superdex 200 3.2/300 column (GE Healthcare) equilibrated in 20 mM HEPES pH 8.0, 150 mM NaCl. 100 µl fractions were collected, proteins were analyzed by SDS-PAGE.

Crosslinking mass spectrometry (XLMS)

For XL-MS, 0.5 mg/ml of the purified complex fractions or of *in vitro* reconstituted protein complexes was crosslinked in 20 mM HEPES pH 8.0, 150 mM NaCl using 0.25 mM DSS (Thermo Fisher) at 25 °C and 500 rpm for 30 min. The reaction was quenched with 50 mM ammonium bicarbonate at 25 °C for 10 min. Samples were evaporated to dryness at 45 °C (Concentrator, Eppendorf), resuspended in 8 M Urea and reduced with 2.5 mM TCEP. Subsequently, samples were alkylated with 5 mM iodoacetamide at room temperature in the dark for 30 min. For digestion, urea was diluted to 1 M by adding 50 mM ammonium bicarbonate and 2 µg Trypsin (Promega) per 100 µg protein. Samples were incubated at 37 °C for 20 hours. Trypsin was inactivated by adding 0.4% (v/v) trifluoroacetic acid. For desalting, samples were loaded on Sep-Pak cartridges (Waters) equilibrated with 5% (v/v) acetonitrile, 0.1% (v/v) formic acid and eluted with 50% (v/v) acetonitrile, 0.1% (v/v) formic acid. To enrich for crosslinked peptides, the samples were separated by SEC. Peptides were resuspended in 30% (v/v) acetonitrile, 0.1% (v/v) trifluoroacetic acid and applied to a Superdex 30 3.2/300 column (GE Healthcare). Fractions containing crosslinked peptides were evaporated to dryness. For MS-analysis samples were resuspended in

5% (v/v) acetonitrile, 0.1% (v/v) TFA. The nano HPLC system used was an UltiMate 3000 RSLC nano system (Thermo Fisher Scientific) coupled to an Orbitrap Fusion Lumos Tribrid mass spectrometer (Thermo Fisher Scientific), equipped with a Proxeon nanospray source (Thermo Fisher Scientific). Peptides were loaded onto a trap column at a flow rate of 25 µl/min using 0.1% TFA as mobile phase. After 10 min, the trap column was switched in line with the analytical column (both columns from Thermo Fisher Scientific). Peptides were eluted at a flow rate of 230 nl/min, and a binary 3 h gradient. The gradient started with 98% mobile phase A (water/formic acid, 99.9%/0.1%, v/v) and 2% mobile phase B (water/acetonitrile/formic acid, 19.92%/80%/0.08%, v/v/v), increased to 35% mobile phase B over 180 min, followed by a 5 min-gradient to 90% mobile phase B. Acquisition was performed in data-dependent mode with a 3 s cycle time. The full scan spectrum was recorded at a resolution of 60 000 in the range of 350-1500 m/z. Precursors with a charge state of +3 to +7 were fragmented. HCD-collision energy was set to 29%. The resolution of MS2-scans recorded in the Orbitrap was 45 000 with a precursor isolation width of 1.0 m/z. Dynamic exclusion was enabled with 30 s exclusion time.

Fragment spectra peak lists were generated from the raw MS-data using the software MSConvert[67] (v 3.0.20105) selecting the peak picking filter. Crosslink search was performed using XiSearch[68] (v 1.7.4) applying the following parameters: 6 ppm MS1-accuracy; 20 ppm MS2-accuracy; DSS-crosslinker with reaction specificity for lysine, serine, threonine, tyrosine and protein N-termini with a penalty of 0.2 (scale 0-1) assigned for serine, threonine and tyrosine; carbamidomethylation of cysteine as a fixed modification; oxidation of methionine as variable modification; tryptic digest with up to four missed cleavages; all other variables were used at default settings. Identified crosslinks were filtered to 5% FDR on link level with the software XiFDR[69] (v 1.4.3.1). For plotting of crosslink data, the in-house software CrossLinkingVisualizer was used[70].

Solubility assay

Hi5 cells were infected for 4 days at 21°C with a baculovirus expressing both UNC-45 WT and myosin variants in the same backbone, as for the “Protein expression” section. Cells were then spinned at 1000G for 15 minutes, weighted and flash-frozen in liquid nitrogen. The pellets were then resuspended in 50 mM Na Phospate pH 8, 300 mM NaCl, 1:5000 benzonase. The volume of buffer for the resuspension was

proportional to the weight of the pellet (5X). The suspension was centrifuged at 20000G for 30 minutes to separate soluble and insoluble fractions. The supernatant of the clear cell lysate was then loaded on a 10% self-cast SDS-PAGE. Quantification of the band intensity was performed with ImageJ, and plotting and statistical analysis (paired t-test) was performed with GraphPad prism.

References

1. Squire, J. M. Architecture and function in the muscle sarcomere. *Curr. Opin. Struct. Biol.* **7,** 247–257 (1997).

2. Hwang, P. M. & Sykes, B. D. Targeting the sarcomere to correct muscle function. *Nat. Rev. Drug Discov.* **14,** 313–328 (2015).

3. Shemesh, N. *et al.* The landscape of molecular chaperones across human tissues reveals a layered architecture of core and variable chaperones. *Nat. Commun.* **12,** 1–16 (2021).

4. Chow, D., Srikakulam, R., Chen, Y. & Winkelmann, D. A. Folding of the striated muscle myosin motor domain. *J. Biol. Chem.* **277,** 36799–36807 (2002).

5. Caldwell, J. T., Melkani, G. C., Huxford, T. & Bernstein, S. I. Transgenic expression and purification of myosin isoforms using the Drosophila melanogaster indirect flight muscle system. *Methods* **56,** 25–32 (2012).

6. Deacon, J. C., Bloemink, M. J., Rezavandi, H., Geeves, M. A. & Leinwand, L. A. Identification of functional differences between recombinant human α and β cardiac myosin motors. *Cell. Mol. Life Sci.* **69,** 2261–2277 (2012).

7. Deshmukh, A. S. *et al.* Deep Proteomics of Mouse Skeletal Muscle Enables Quantitation of Protein Isoforms, Metabolic Pathways, and Transcription Factors. *Mol. Cell. Proteomics* **14,** 841 (2015).

8. Kachur, T. & Pilgrim, D. Myosin Assembly, Maintenance and Degradation in Muscle: Role of the Chaperone UNC-45 in Myosin Thick Filament Dynamics. *Int. J. Mol. Sci.* **9,** 1863–1875 (2008).

9. Epstein, H. F. & Thomson, J. N. Temperature-sensitive mutation affecting myofilament assembly in Caenorhabditis elegans. *Nature* **250,** 579–580 (1974).

10. Barral, J. M., Bauer, C. C., Ortiz, I. & Epstein, H. F. Unc-45 mutations in Caenorhabditis elegans implicate a CRO1/She4p-like domain in myosin assembly. *J. Cell Biol.* **143,** 1215–1225 (1998).

11. Barral, J. M., Hutagalung, A. H., Brinker, A., Hartl, F. U. & Epstein, H. F. Role of the myosin assembly protein UNC-45 as a molecular chaperone for myosin. *Science (80-.).* **295,** 669–671 (2002).

12. Lee, C. F. *et al.* Drosophila UNC-45 accumulates in embryonic blastoderm and

in muscles, and is essential for muscle myosin stability. *J. Cell Sci.* **124,** 699–705 (2011).

13. Gazda, L. *et al.* The myosin chaperone UNC-45 is organized in tandem modules to support myofilament formation in C. elegans. *Cell* **152,** 183–195 (2013).

14. Melkani, G. C., Bodmer, R., Ocorr, K. & Bernstein, S. I. The UNC-45 Chaperone Is Critical for Establishing Myosin-Based Myofibrillar Organization and Cardiac Contractility in the Drosophila Heart Model. *PLoS One* **6,** e22579 (2011).

15. Bernick, E. P., Zhang, P.-J. & Du, S. Knockdown and overexpression of Unc-45b result in defective myofibril organization in skeletal muscles of zebrafish embryos. *BMC Cell Biol.* **11,** 70 (2010).

16. Dafsari, H. S. *et al.* Bi-allelic mutations in uncoordinated mutant number-45 myosin chaperone B are a cause for congenital myopathy. *Acta Neuropathol. Commun.* **7,** 1–5 (2019).

17. Donkervoort, S. *et al.* Pathogenic Variants in the Myosin Chaperone UNC-45B Cause Progressive Myopathy with Eccentric Cores. *Am. J. Hum. Genet.* **23,** 30 (2020).

18. Lee, C. F., Melkani, G. C. & Bernstein, S. I. The UNC-45 Myosin Chaperone. From Worms to Flies to Vertebrates. *Int. Rev. Cell Mol. Biol.* **313,** 103–144 (2014).

19. Scheufler, C. *et al.* Structure of TPR domain-peptide complexes: Critical elements in the assembly of the Hsp70-Hsp90 multichaperone machine. *Cell* **101,** 199–210 (2000).

20. Hellerschmied, D. *et al.* UFD-2 is an adaptor-assisted E3 ligase targeting unfolded proteins. *Nat. Commun.* **9,** 484 (2018).

21. Etard, C., Roostalu, U. & Strähle, U. Shuttling of the chaperones Unc45b and Hsp90a between the A band and the Z line of the myofibril. *J. Cell Biol.* **180,** 1163–1175 (2008).

22. Landsverk, M. L. *et al.* The UNC-45 chaperone mediates sarcomere assembly through myosin degradation in Caenorhabditis elegans. *J. Cell Biol.* **177,**

(2007).

23. Erbse, A., Mayer, M. P. & Bukau, B. Mechanism of substrate recognition by Hsp70 chaperones. *Biochem. Soc. Trans.* **32,** 617–621 (2004).

24. Clerico, E. M., Tilitsky, J. M., Meng, W. & Gierasch, L. M. How Hsp70 molecular machines interact with their substrates to mediate diverse physiological functions. *Journal of Molecular Biology* **427,** 1575–1588 (2015).

25. Scheibel, T., Weikl, T. & Buchner, J. Two chaperone sites in Hsp90 differing in substrate specificity and ATP dependence. *Proc. Natl. Acad. Sci.* **95,** 1495–1499 (1998).

26. Joachimiak, L. A., Walzthoeni, T., Liu, C. W., Aebersold, R. & Frydman, J. The structural basis of substrate recognition by the eukaryotic chaperonin TRiC/CCT. *Cell* **159,** 1042 (2014).

27. Rao, D. S. *et al.* Reductions in ATPase activity, actin sliding velocity, and myofibril stability yield muscle dysfunction in Drosophila models of myosin-based Freeman–Sheldon syndrome. *Mol. Biol. Cell* **30,** 30–41 (2019).

28. Toydemir, R. M. *et al.* Mutations in embryonic myosin heavy chain (MYH3) cause Freeman-Sheldon syndrome and Sheldon-Hall syndrome. *Nat. Genet.* **38,** 561–565 (2006).

29. Hellerschmied, D. *et al.* Molecular features of the UNC-45 chaperone critical for binding and folding muscle myosin. *Nat. Commun.* **10,** 4781 (2019).

30. Das, A. *et al.* A heterotypic assembly mechanism regulates CHIP E3 ligase activity. *EMBO J.* **41,** e109566 (2022).

31. Gaziova, I. *et al.* Mutational Analysis of the Structure and Function of the Chaperoning Domain of UNC-45B. *Biophys. J.* **119,** 780–791 (2020).

32. Shi, H. & Blobel, G. UNC-45/CRO1/She4p (UCS) protein forms elongated dimer and joins two myosin heads near their actin binding region. *Proc. Natl. Acad. Sci.* **107,** 21382–21387 (2010).

33. Huber, A. H., Nelson, W. J. & Weis, W. I. Three-dimensional structure of the armadillo repeat region of β-catenin. *Cell* **90,** 871–882 (1997).

34. Toydemir, R. M. *et al.* Mutations in embryonic myosin heavy chain (MYH3) cause Freeman-Sheldon syndrome and Sheldon-Hall syndrome. *Nat. Genet.*

38, 561–565 (2006).

35. Quintana-Gallardo, L. *et al.* The cochaperone CHIP marks Hsp70- and Hsp90-bound substrates for degradation through a very flexible mechanism. *Sci. Rep.* **9,** 1–16 (2019).

36. Noddings, C. M., Yu-Ruei Wang, R. & Agard, D. A. GR chaperone cycle mechanism revealed by cryo-EM: reactivation of GR by the 1 GR:Hsp90:p23 client-maturation complex 2. doi:10.1101/2020.09.12.294975

37. Karagöz, G. E. *et al.* Hsp90-tau complex reveals molecular basis for specificity in chaperone action. *Cell* **156,** 963–974 (2014).

38. Saio, T., Guan, X., Rossi, P., Economou, A. & Kalodimos, C. G. Structural basis for protein antiaggregation activity of the trigger factor chaperone. *Science* **344,** (2014).

39. Huang, C. & Kalodimos, C. G. Structures of Large Protein Complexes Determined by Nuclear Magnetic Resonance Spectroscopy. *https://doi.org/10.1146/annurev-biophys-070816-033701* **46,** 317–336 (2017).

40. Jiang, Y., Rossi, P. & Kalodimos, C. G. Structural basis for client recognition and activity of Hsp40 chaperones. *Science* **365,** 1313–1319 (2019).

41. Verba, K. A. *et al.* Atomic structure of Hsp90-Cdc37-Cdk4 reveals that Hsp90 traps and stabilizes an unfolded kinase. *Science (80-.).* **352,** 1542–1547 (2016).

42. Balchin, D., Miličić, G., Strauss, M., Hayer-Hartl, M. & Hartl, F. U. Pathway of Actin Folding Directed by the Eukaryotic Chaperonin TRiC. *Cell* **174,** 1507–1521.e16 (2018).

43. Gestaut, D. *et al.* The Chaperonin TRiC/CCT Associates with Prefoldin through a Conserved Electrostatic Interface Essential for Cellular Proteostasis. *Cell* **177,** 751–765.e15 (2019).

44. Hammond, C. M., Strømme, C. B., Huang, H., Patel, D. J. & Groth, A. Histone chaperone networks shaping chromatin function. *Nat. Rev. Mol. Cell Biol. 2017 183* **18,** 141–158 (2017).

45. Saschenbrecker, S. *et al.* Structure and Function of RbcX, an Assembly Chaperone for Hexadecameric Rubisco. *Cell* **129,** 1189–1200 (2007).

46. Hou, Z. *et al.* DnaJC7 binds natively folded structural elements in tau to inhibit amyloid formation. *Nat. Commun. 2021 121* **12,** 1–17 (2021).

47. Koppole, S., Smith, J. C. & Fischer, S. Simulations of the Myosin II Motor Reveal a Nucleotide-state Sensing Element that Controls the Recovery Stroke. *J. Mol. Biol.* **361,** 604–616 (2006).

48. Koppole, S., Smith, J. C. & Fischer, S. The Structural Coupling between ATPase Activation and Recovery Stroke in the Myosin II Motor. *Structure* **15,** 825–837 (2007).

49. Bujalowski, P. J., Nicholls, P., Garza, E. & Oberhauser, A. F. The central domain of UNC-45 chaperone inhibits the myosin power stroke. **8,** 41–48 (2018).

50. Vera, C. D. *et al.* Myosin motor domains carrying mutations implicated in early or late onset hypertrophic cardiomyopathy have similar properties. *J. Biol. Chem.* **294,** 17451–17462 (2019).

51. Adhikari, A. S. *et al.* β-Cardiac myosin hypertrophic cardiomyopathy mutations release sequestered heads and increase enzymatic activity. *Nat. Commun.* **10,** 1–10 (2019).

52. Anderson, R. L. *et al.* Deciphering the super relaxed state of human β-cardiac myosin and the mode of action of mavacamten from myosin molecules to muscle fibers. *Proc. Natl. Acad. Sci.* **115,** E8143–E8152 (2018).

53. Meister-Broekema, M. *et al.* Myopathy associated BAG3 mutations lead to protein aggregation by stalling Hsp70 networks. *Nat. Commun.* **9,** 5342 (2018).

54. Sarparanta, J. *et al.* Mutations affecting the cytoplasmic functions of the co-chaperone DNAJB6 cause limb-girdle muscular dystrophy. *Nat. Genet.* **44,** 450–455 (2012).

55. Fan, G. C. & Kranias, E. G. Small heat shock protein 20 (HspB6) in cardiac hypertrophy and failure. *Journal of Molecular and Cellular Cardiology* **51,** 574–577 (2011).

56. Ranek, M. J., Stachowski, M. J., Kirk, J. A. & Willis, M. S. The role of heat shock proteins and co-chaperones in heart failure. *Philosophical Transactions of the Royal Society B: Biological Sciences* **373,** (2018).

57. Alexander, A. G., Marfil, V. & Li, C. Use of Caenorhabditis elegans as a model to study Alzheimer's disease and other neurodegenerative diseases. *Front. Genet.* **5,** (2014).

58. Cooper, J. F. *et al.* Activation of the mitochondrial unfolded protein response promotes longevity and dopamine neuron survival in Parkinson's disease models. *Sci. Rep.* **7,** (2017).

59. Baskoylu, S. N. *et al.* Disrupted autophagy and neuronal dysfunction in C. elegans knockin models of FUS amyotrophic lateral sclerosis. *Cell Rep.* **38,** 110195 (2022).

60. Chen, I., Dorr, B. M. & Liu, D. R. A general strategy for the evolution of bond-forming enzymes using yeast display. doi:10.1073/pnas.1101046108/-/DCSupplemental

61. McCoy, A. J. *et al.* Phaser crystallographic software. *J. Appl. Crystallogr.* **40,** 658–674 (2007).

62. Brünger, A. T. *et al.* Crystallography & NMR system: A new software suite for macromolecular structure determination. *Acta Crystallogr. Sect. D Biol. Crystallogr.* **54,** 905–921 (1998).

63. Jones, T. A., Zou, J. -Y, Cowan, S. W. & Kjeldgaard, M. Improved methods for building protein models in electron density maps and the location of errors in these models. *Acta Crystallogr. Sect. A* **47,** 110–119 (1991).

64. Edgar, R. C. MUSCLE: Multiple sequence alignment with high accuracy and high throughput. *Nucleic Acids Res.* **32,** 1792–1797 (2004).

65. Waterhouse, A. M., Procter, J. B., Martin, D. M. A., Clamp, M. & Barton, G. J. Jalview Version 2-A multiple sequence alignment editor and analysis workbench. *Bioinformatics* **25,** 1189–1191 (2009).

66. Ahel, J. *et al.* Moyamoya disease factor RNF213 is a giant E3 ligase with a dynein-like core and a distinct ubiquitin-transfer mechanism. *Elife* **9,** (2020).

67. Chambers, M. C. *et al.* A cross-platform toolkit for mass spectrometry and proteomics. *Nature Biotechnology* **30,** 918–920 (2012).

68. Giese, S. H., Fischer, L. & Rappsilber, J. A study into the collision-induced dissociation (CID) behavior of cross-linked peptides. *Mol. Cell. Proteomics* **15,**

1094–1104 (2016).

69. Fischer, L. & Rappsilber, J. Quirks of Error Estimation in Cross-Linking/Mass Spectrometry. doi:10.1021/acs.analchem.6b03745

70. Ahel, J. GitHub - ClausenLab-ViennaBioCenter/CrossLinkingVisualizer.

SUPPLEMENTARY INFORMATION

UNC-45 assisted myosin folding depends on a conserved FX_3HY motif implicated in Freeman Sheldon Syndrome

Antonia Vogel[1,4], Renato Arnese[1,4], Ricardo M. Gudino Carrillo[1,2], Daria Sehr, Andrzej Bylicki[11], Anton Meinhart[1], Tim Clausen[1,3,*]

[1]Research Institute of Molecular Pathology, Vienna BioCenter, Vienna, Austria

[2]Current address: Vienna BioCenter Core Facilities, Vienna, Austria

[3]Vienna BioCenter Core Facilities, Vienna, Austria

[3]Medical University, Vienna, Austria

[4]These authors contributed equally

*Correspondence: tim.clausen@imp.ac.at

The file contains the Supplementary Figurs S1-S9.

Supplementary Figures

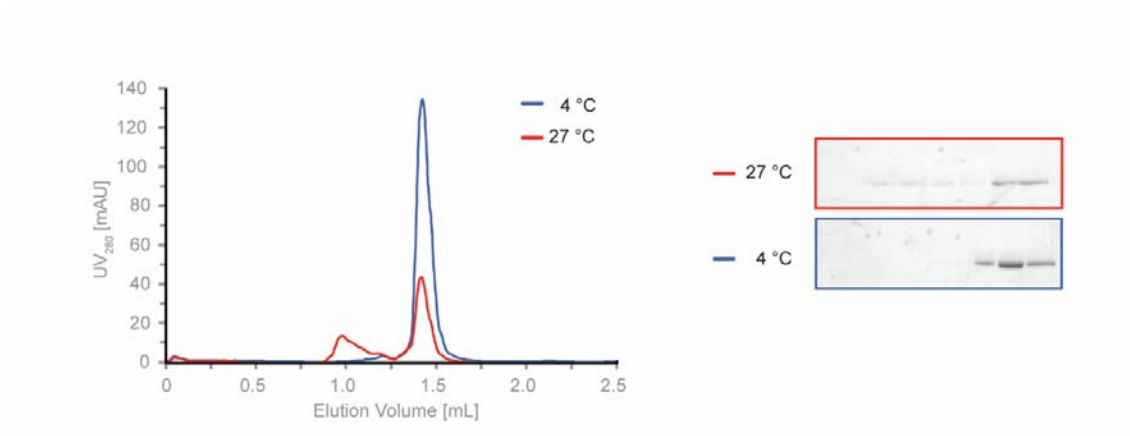

Supp. Fig. 1 Recombinant myosin unfolds at high temperatures

SEC of recombinant myosin incubated at 4 °C (folded) and at 27 °C (partially unfolded). SDS-PAGE of the peaks is shown on the right.

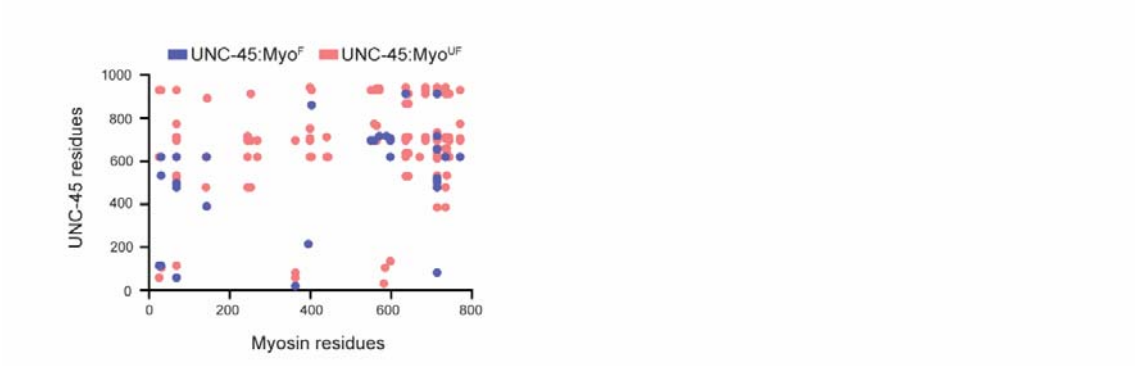

Supp. Fig 2 UNC-45:Myo^{F} and UNC-45:Myo^{UF} show distinct crosslink patterns compatible with folded and unfolded myosin

Plot of interlinks comparing complexes with UNC-45 containing intact (blue) or damaged (red) myosin. Links have been filtered to FDR ≤ 5%.

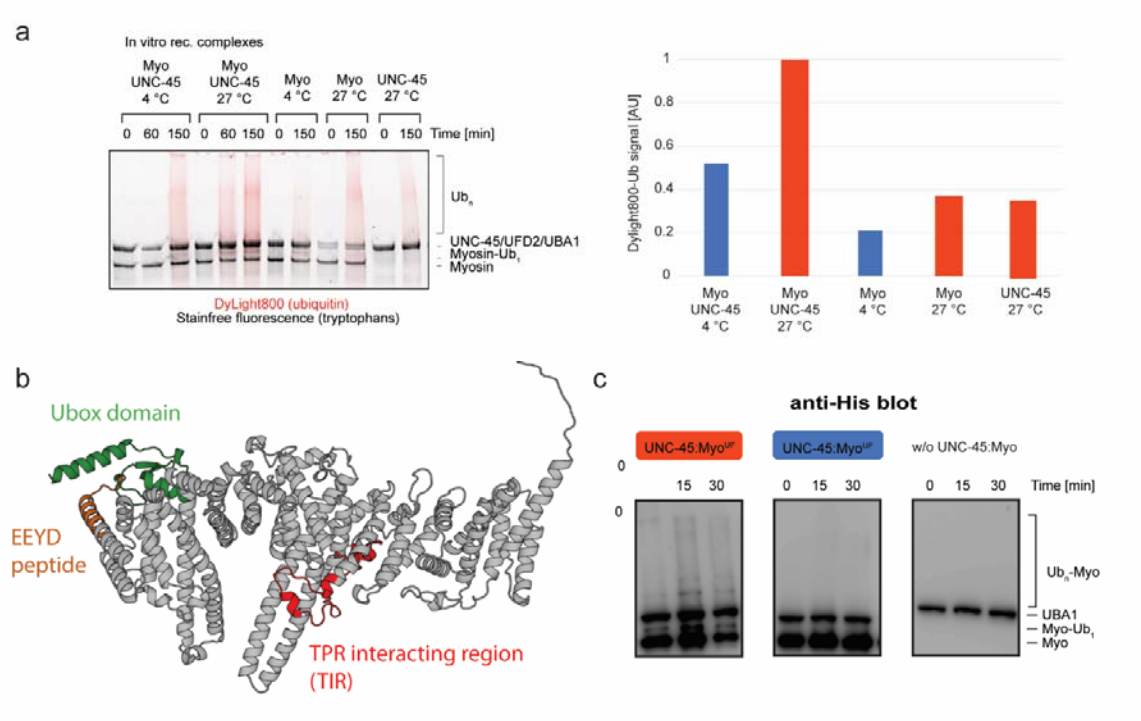

Supp. Fig. 3 UFD-2 specifically targets damaged myosin for ubiquitination

(a) Left: UFD-2-mediated ubiquitination of *in vitro* reconstituted UNC-45:myosin complexes and UNC-45 or myosin alone performed at 4 °C and 27 °C. SDS-PAGE gels with signals of stain-free fluorescence (total protein) and DyLight800 (ubiquitin) have been overlayed. Right: Quantification of Ub_n after 150 minutes using DyLight800 signal. **(b)** AlphaFold model of UFD2 with Ubox (green) and the TPR-interacting region (red) identified XLMS (**Fig. 2c**). The peptide containing the internal EEYD is labeled in orange. **(c)** Anti-HIS Western Blot of purified UNC-45:myosin complexes after ubiquitination with UFD-2. Myosin and UBA1 (E1) are expressed with a His-tag thus probing with an anti-His antibody distinguishes myosin- from UNC-45-ubiquitination.

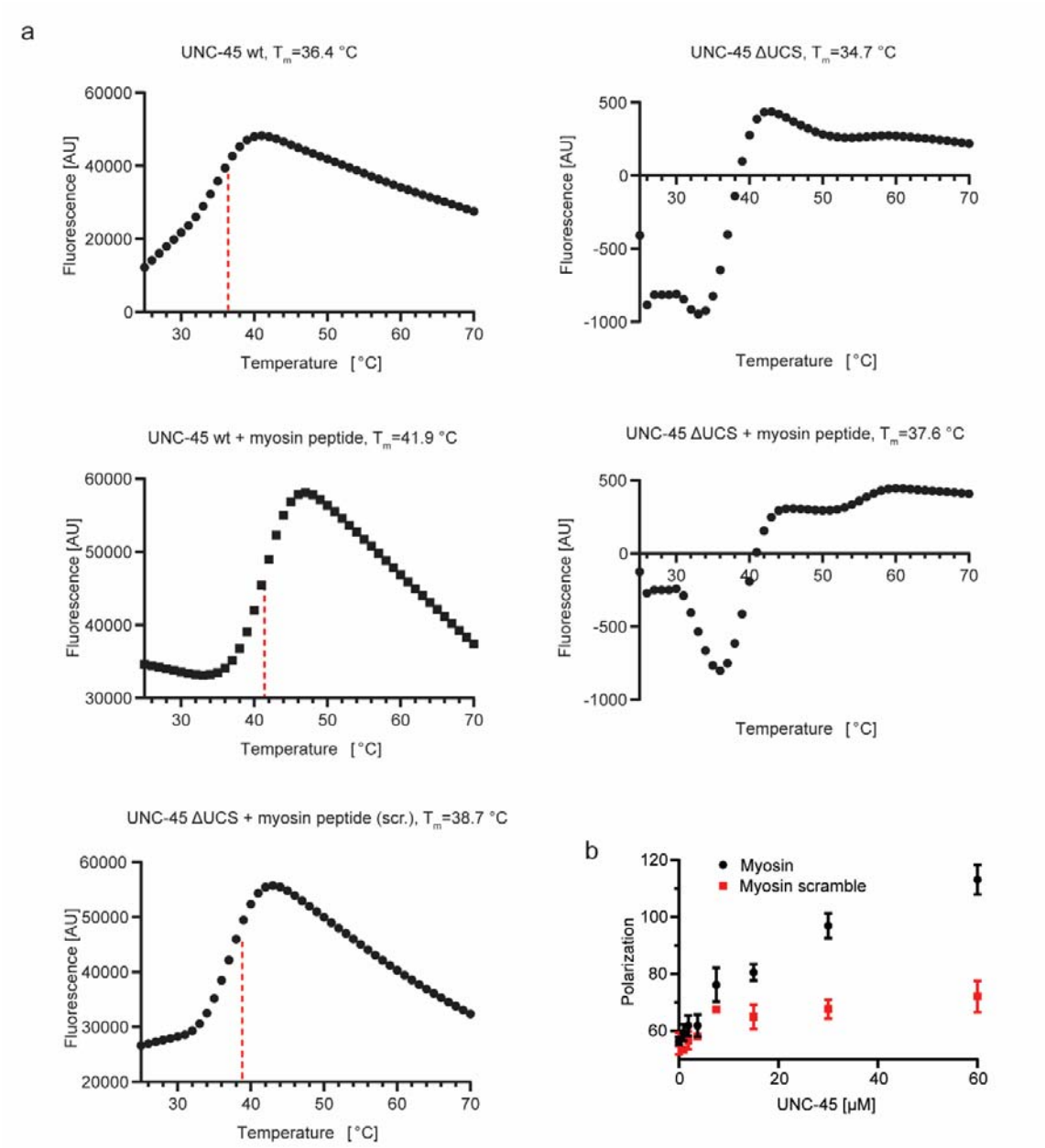

Supp. Fig. 4 A discrete myosin peptide specifically binds to the UNC-45 UCS domain

(a) Selected, representative melting curves of thermal shift assays. Red dashed lines indicate the determined melting temperatures (T_m). **(b)** Fluorescence anisotropy of myosin peptides. For measurements the minimal motif shown in figure **Fig. 3b** was used. Mean and SD of 3 technical replicate are shown.

a

```
KlSHE4/1-663     1 ------------------MNKVWDRIVGS--------DSADAQSVLKERCSS---PKDVTD------------  32
ScSHE4/1-789     1 MPLCEKGNDPIDSSTIDSLCAAFDKTLKSTPDVQKYNDAINTIFQLRQKSESGKMPADLTNSEALKDRQKIEE  73

KlSHE4/1-663    33 ---------------LLHVIQN------------WTSEIH-----------------------NNGEETRC--  53
ScSHE4/1-789    74 ILTRSYQDHSESRVHLSKLIQNDIPFALNLFEILSRSSIHVFVGCFSNKDATIALLNELQIRIHYGEDTHVTY 146

KlSHE4/1-663    54 --WKCVPMLAGYVKDWGQLEFLCRRILLRSSIQEIRPLLLVTMKSLMSNHSDNTEQKCGNILQQLLIEAEEDS 124
ScSHE4/1-789   147 LLSIILQLLNKFKYNFKEVRFLVKELILRISEDEVKSMMLIIFAELQSSFQKDFDKAVVDFMSSLIVEAEIDV 219

KlSHE4/1-663   125 GNVSLRLLVDAMSLVFPICLGVCRDMFLSTDFQDILTRNLNSSADDEHLVNGALRLLAVSCIDEAVRRFIAEH 197
ScSHE4/1-789   220 GNDPLSIIVKTLSELYPSLTTLCSEIFLTKGLSKLFKKRV-FEEQDLQFTKELLRLLSSACIDETMRTYITEN 291

KlSHE4/1-663   198 YLKTLQQSFKVEKYKVLTALVLIKIWSFTKIEKETLNSCINLFIDSLSNG------------------ENIEI 252
ScSHE4/1-789   292 YLQLLERSLNVEDVQIYSALVLVKTWSFTKLTCINLKQLSEIFINAISRRIMPKIENVNESAVKLEEVPKVEM 364

KlSHE4/1-663   253 NTEALAYLTLKPSVRVLLRGNGDVCLKIIELIKSQDTTPTDLYGLLIILANVSEHPSQNE---DTVDKLK--A 320
ScSHE4/1-789   365 SVEALAYLSLKASVKIMIRSNESFTEILLTMIKSQKMTHC-LYGLLVIMANLSTLPEESNGSSQSINDLKNYA 436

KlSHE4/1-663   321 SLKTNQEKNDEPTLENVKDIEEFNRDYIIDLDLIGSLKS--IKLSTSSYNQAIRIIYNVTRDKTQISECVKQG 391
ScSHE4/1-789   437 DLKGPGADKVGAEKESKEDILLFNEKYILRTELISFLKREMHNLSPNCKQQVVRVIYNITRSKNFIPQCISQG 509

KlSHE4/1-663   392 AGLMLLVFLAQKRNLSKDEWYLLSIRALSKTLIYVNPETAFSKYSPLSAAPFLFENLPLP---NDNAL-SELQ 460
ScSHE4/1-789   510 GTTIILEYLANKQDIG-EPIRILGCRALTRMLIFTNPGLIFKKYSALNAIPFLFELLPRSTPVDDNPLHNDEQ 581

KlSHE4/1-663   461 FTQLDTYEALLALTNLAT--INQGVDLGKIILSNAQYWDSIENLLLDSSVRIQRSTLELISNLMSNPMAISAK 531
ScSHE4/1-789   582 IKLTDNYEALLALTNLASSETSDGEEVCKHIVSTKVYWSTIENLMLDENVPLQRSTLELISNMMSHPLTIAAK 654

KlSHE4/1-663   532 FFCFENPKSAQNFEILVKLLELHDIQSQRAVAAIFANIASTVPFICKELSEKRNLIETAIRVFKTQNTDTDLR 604
ScSHE4/1-789   655 FFNLENPQSLRNFNILVKLLQLSDVESQRAVAAIFANIATTIPLIAKELLTKKELIENAIQVFADQIDDIELR 727

KlSHE4/1-663   605 IRLLVLLSSIF-----NANAHAVACVKNDEEFVKELQKYRNTPSQKDPLTPELSKE---ILSLINLE      663
ScSHE4/1-789   728 QRLLMLFFGLFEVIPDNGTNEVYPLLQENQKLKDAL----NMSLKRGDSGPEFSAAIPVILAKIKV-       789
```

b

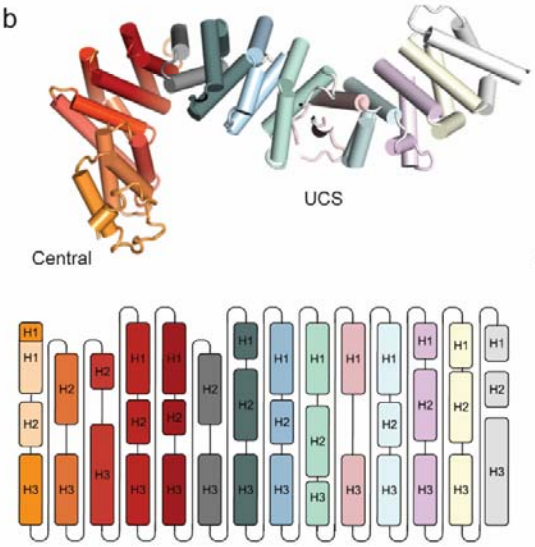

c

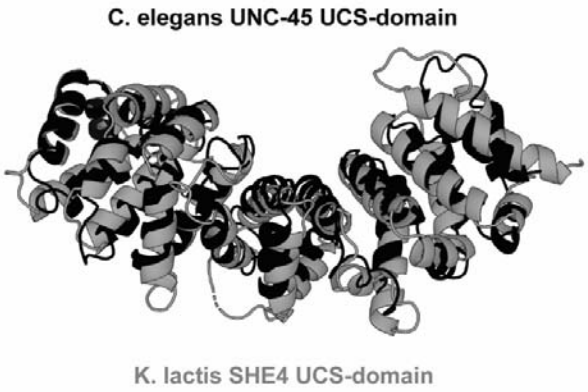

Supp. Fig. 5 *K. lactis* SHE4 crystal structure

(a) Alignment of SHE4 comparing the sequences from the *K. lactis* chaperone used in this study and *S. cerevisiae* that has been described previously in Shi & Blobel, 2010. **(b)** ARM repeats of *K. lactis* SHE4 colored according to sequence, highlighting irregular repeats at functional important sites (e.g. in center of UCS domain, providing en-bloc flexibility to accommodate substrate). **(c)** Superposition of *K. lactis* SHE4 (grey) and *C. elegans* UNC-45 (PDB: 4i2z, light blue) UCS domains, that can be aligned with an RMS deviation of 3.8 Å over 321 Cα-atoms

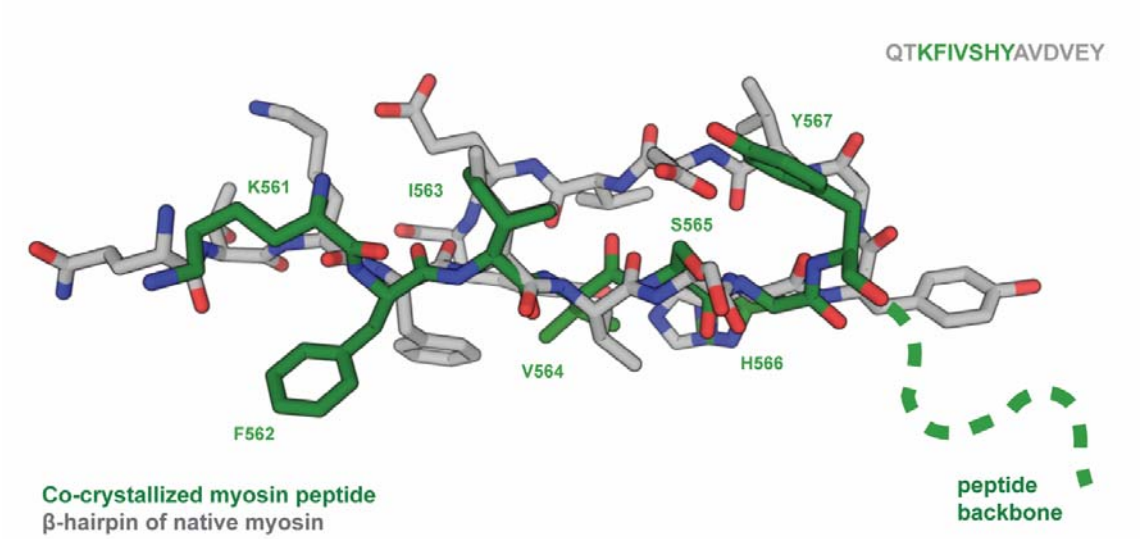

Supp, Fig. 6 *K. lactis* SHE4 binds the myosin peptide in an extended conformation

Structural alignment of the co-crystallized myosin peptide (green) and the native myosin β-hairpin loop of myo4 (grey) reveals different backbone conformations. Whereas in native myosin, Tyr567 is the first residue of a β-hairpin, the same tyrosine adopts a different backbone conformation in the chaperone-bound state that is consistent with an extended peptide stretch, as indicated schematically (dotted backbone line).

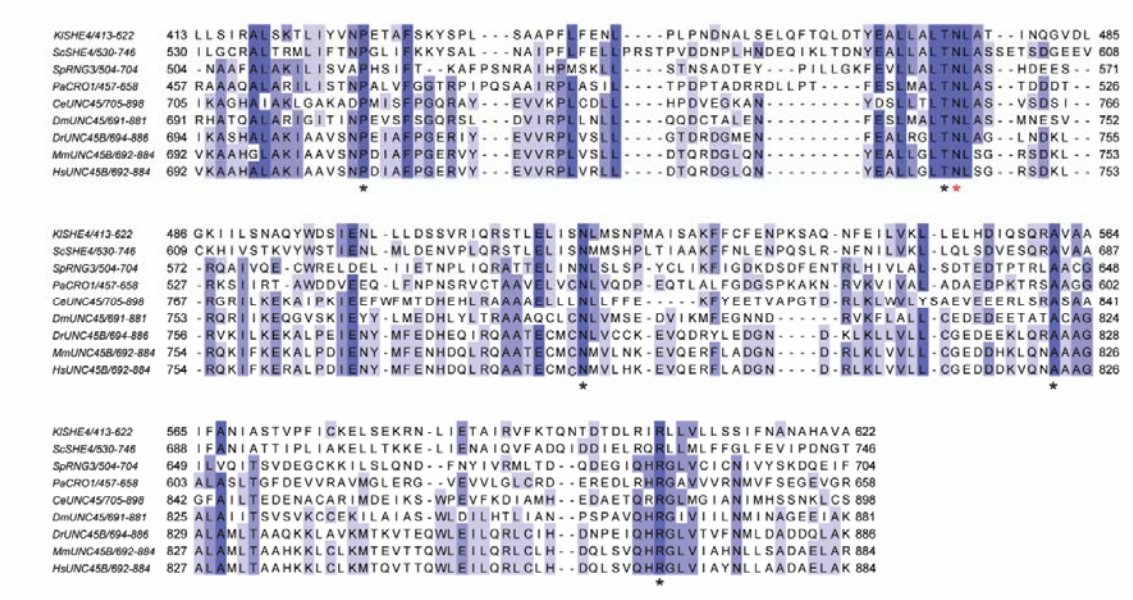

Supp. Fig. 7 *K. lactis* SHE4 binds the myosin peptide via a conserved interface

Sequence alignment of the myosin binding region of UCS-proteins from selected species. Strictly conserved residues that are involved in myosin binding are marked with an asterisk (Asn475 used to generate the N457A mutant in the present study highlighted with red asterisk). Residues are coloured in shades of blue according to percentage identity with dark blue >80% and white <40%.

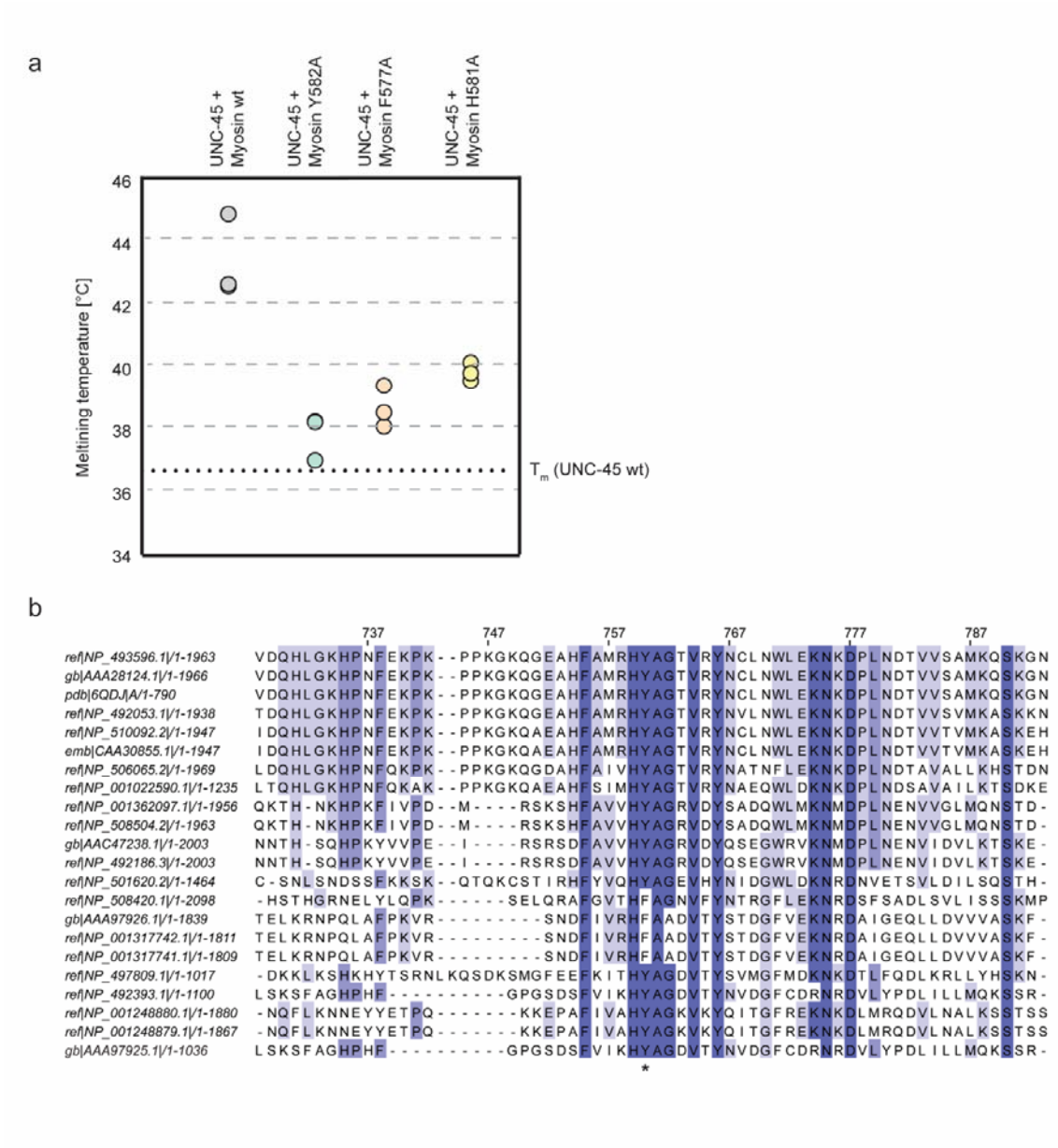

Supp. Fig. 8 Validation of the FX_3HY-motif for UNC-45 binding and conservation among *C. elegans* myosin isoforms

(a) Thermal shift assays comparing melting temperatures of UNC-45 in presence of the WT myosin peptide versus different mutants of the FX_3HY-motif. Dotted line indicates the melting temperature of WT UNC-45 in absence of peptides as observed in **Fig. 3c**. **(b)** Conservation of FX3HY-motif in *C. elegans* myosin isoforms. Position 582 is indicated with an asterisk, displaying either Y or F.

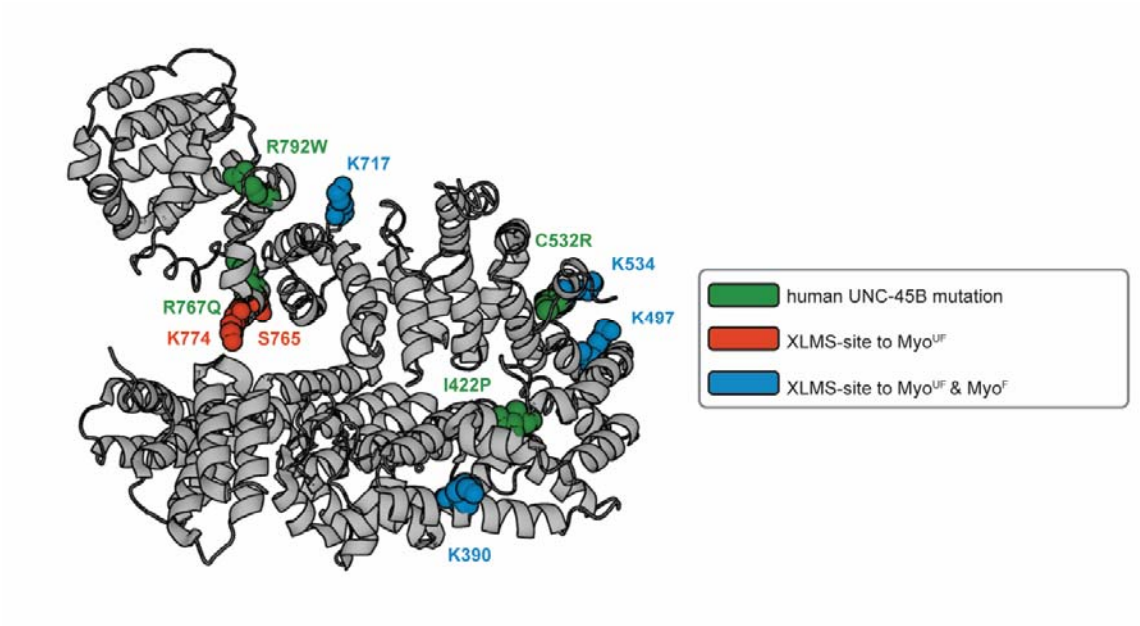

Supp. Fig. 9 Comparison of crosslink sites to myosin and human point mutation causing myopathies mapped on the UNC-45 structure

Mapping of residues on the *C. elegans* UNC-45 structure (PDB: 4i2z) of which point mutations have been linked to human myopathies (green) and where interlinks with myosin (red and blue) have been found.